New Phytologist

Suppression of xylan endotransglycosylase PtxtXyn10A affects cellulose microfibril angle in secondary wall in aspen wood

Journal:	*New Phytologist*
Manuscript ID:	NPH-MS-2014-17912.R1
Manuscript Type:	MS - Regular Manuscript
Date Submitted by the Author:	n/a
Complete List of Authors:	Debra-Maceluch, Marta; Swedish University of Agricultural Sciences, Department of Forest Genetics and Plant Physiology Awano, Tatsuya; Kyoto University, Division of Forest and Biomaterials Science Takahashi-Schmidt, Junko; Swedish University of Agricultural Sciences, Department of Forest Genetics and Plant Physiology Lucenius, Jessica; University of Helsinki, Department of Physics Ratke, Christine; Swedish University of Agricultural Sciences, Deprtament of Forest Genetics and Plant Physiology; Swedish University of Agricultural Sciences, Department of Forest Genetics and Plant Physiology Kontro, Inkeri; University of Helsinki, Department of Physics Busse-Wicher, Marta; University of Cambridge, Department of Biochemistry Kosik, Ondrej; University of Cambridge, Department of Biochemistry Tanaka, Ryo; Kyoto University, Division of Forest and Biomaterials Science Winzéll, Anders; Royal Institute of Technology, School of Biotechnology Kallas, Åsa; Royal Institute of Technology, School of Biotechnology Leśniewska, Joanna; University of Białystok, Department of Botany Berthold, Fredrik; Innventia, Innventia AB Immerzeel, Peter; Swedish University of Agricultural Sciences, Deprtament of Forest Genetics and Plant Physiology Teeri, Tuula; Aalto University , ; Royal Institute of Technology, School of Biotechnology Ezcurra, Ines; Royal Institute of Technology, School of Biotechnology; KTH, Biotechnology Dupree, Paul; University of Cambridge, Department of Biochemistry Serimaa, Ritva; University of Helsinki, Department of Physics Mellerowicz, Ewa; Swedish University of Agricultural Sciences, Forest Genetics and Plant Physiology; Swedish University of Agricultural Sciences, Department of Forest Genetics and Plant Physiology
Key Words:	Populus, hybrid aspen, secondary cell wall, wood formation, xylanase, xylan endotransglycosylase, cellulose microfibril angle, growth stresses

Suppression of xylan endotransglycosylase *PtxtXyn10A* affects cellulose microfibril angle in secondary wall in aspen wood

Marta Derba-Maceluch[1]*, Tatsuya Awano[1,2]*, Junko Takahashi[1], Jessica Lucenius[3,8], Christine Ratke[1], Inkeri Kontro[3], Marta Busse-Wicher[4], Ondrej Kosik[4,9], Ryo Tanaka[2], Anders Winzéll[5], Åsa Kallas[5], Joanna Leśniewska[1,6], Fredrik Berthold[7], Peter Immerzeel[1], Tuula T. Teeri[5,10], Ines Ezcurra[5], Paul Dupree[4], Ritva Serimaa[3], and Ewa J. Mellerowicz[1]‡

[1] Department of Forest Genetics and Plant Physiology, SLU, Umeå Plant Science Centre (UPSC), Umeå, Sweden

[2] Division of Forest and Biomaterials Science, Graduate School of Agriculture, Kyoto University, Kyoto, Japan

[3] Department of Physics, University of Helsinki, PO Box 64, FIN-00014 Helsinki, Finland

[4] Department of Biochemistry, University of Cambridge, Tennis Court Road, CB2 1QW, Cambridge, UK

[5] School of Biotechnology, Royal Institute of Technology (KTH), Stockholm, Sweden

[6] Department of Botany, University of Białystok, Swierkowa 20 b, 15950 Białystok, Poland

[7] INNVENTIA AB, Drottning Kristinas väg 61, Stockholm, Sweden

[8] Present address: Aalto University, School of Chemical Technology, Department of Forest Products Technology, P.O. Box 16300, FI-00076 Aalto, Finland

[9] Present address: Centre for Crop Genetic Improvement, Department of Plant Biology and Crop Science, Rothamsted Research, West Common, Harpenden, Herts AL5 2JQ, UK

[10] Present address: Aalto University, P.O.Box 17800, FI-00076 Aalto, Finland

* These authors contributed equally to this work.

‡**Author for correspondence**
Ewa J. Mellerowicz
Tel: +46 90 786 8367
Email: ewa.mellerowicz@slu.se

Introduction: 651 words.
Materials and Methods: 1974
Results: 2659
Discussion: 1184
Acknowledgements: 68

Figures 1 – 9. Figures 1, 5 and 9 should be published in colour.
Tables 1 – 2.
Supporting Information : Fig. S1 – S6, Method S1, Tables S1 – S6.

Financial sources: Formas (including HemiPop and FuncFiber), Swedish Research Council (VR), Swedish Governmental Agency for Innovation Systems (VINNOVA), Swedish Center for Biomimetic Fiber Engineering (funded by the Knut & Alice Wallenberg Foundation and the Foundation for Strategic Research), European projects EDEN (QLK5-CT-2001-00443) and RENEWALL, FORE, Bio4Energy, Wood Ultrastructure Research Centre, SamNordisk Skogsforskning (project no. 107), Japan Society for the Promotion of Science (JSPS KAKENHI Grant Number 24580243) and the Academy of Finland (1127759).

Summary

- Certain xylanases from family GH10 are highly expressed during secondary wall deposition, but their function is unknown. We carried out functional analyses of the secondary-wall specific *PtxtXyn10A* in hybrid aspen (*Populus tremula* L. x *tremuloides* Michx.).
- *PtxtXyn10A* function was analysed by expression studies, overexpression in Arabidopsis protoplasts and by downregulation in aspen.
- *Ptxt*Xyn10A overexpression in Arabidopsis protoplasts resulted in increased xylan endotransglycosylation rather than hydrolysis. In aspen, the enzyme was found to be proteolytically processed to a 68 kDa peptide and residing in cell wall. Its downregulation resulted in a corresponding decrease in xylan endotransglycosylase activity and no change in xylanase activity. This did not alter xylan molecular weight or its branching pattern but affected the cellulose-microfibril angle in wood fibres, increased primary growth (stem elongation, leaf formation and enlargement) and reduced the tendency to form tension wood. Transcriptomes of transgenic plants showed downregulation of tension wood related genes and changes in stress-responsive genes.
- The data indicate that *Ptxt*Xyn10A acts as a xylan endotransglycosylase and its main function is to release tensional stresses arising during secondary wall deposition. Furthermore, they suggest that regulation of stresses in secondary walls plays a vital role in plant development.

Key words: *Populus,* hybrid aspen, secondary cell wall, wood formation, xylanase, xylan endotransglycosylase, cellulose microfibril angle, growth stresses

Introduction

Xylans are among most abundant polysaccharides found in nature (Ebringerová & Heinze, 2000; Scheller & Ulvskov, 2010). They are polymers with a β-1,4-D-xylopyranose backbone and include homoxylans and heteroxylans, such as arabinoxylans, glucuronoxylans and glucuronoarabinoxylans. Glucuronoxylans are abundant in the secondary walls of dicotyledonous species, where they are the main hemicellulose, comprising roughly one fourth of wood biomass, whereas arabinoxylans and glucuronoarabinoxylans are found in type II primary cell walls of grasses and secondary walls of conifers, respectively. Small amounts of glucuronoarabinoxylans are also present in the primary cell walls of eudicots and lower vascular plants (Darvill *et al.*, 1980; McCartney *et al.*, 2006; Brummell & Schröder, 2009). The importance of understanding the biosynthesis and modification of xylans in plants is emphasised by the increasing significance of plant biomass as a potential source of renewable energy and use of hemicelluloses as food additives and pharmacologically active ingredients (Bevan & Franssen, 2006).

In *Populus* wood, xylans have a backbone of approximately 100 units long with side chains of 4-*O*-methyl-α-D-glucuronic acid (Me-GlcUA) at *O*-2 in approximately every tenth xylose residue (Timell, 1967; Teleman *et al.*, 2000). In addition, approximately 50% of the xylose residues are *O*-acetylated at the C-2, C-3 or both positions (Naran *et al.*, 2009). An oligosaccharide containing β-D-Xyl-(1,4)-β-D-Xyl-(1,3)-α-L-Rha-(1,2)-α-D-GalUA-(1,4)-D-Xyl resides at the reducing end of the *Populus* xylan, similar to found in other eudicots and conifers (Lee *et al.*, 2011). In secondary walls, glucuronoxylans are thought to interact with lignin via ester bonding to GlcUA and Me-GlcUA (Imamura *et al.*, 1994; Spániková & Biely, 2006; Spániková *et al.*, 2007; Li *et al.*, 2007).

The biosynthesis of xylan involves several different classes of glycosyltransferases (GTs) that make up the backbone, the reducing end sequence and different side chains (recently reviewed by Rennie & Scheller, 2014). These enzymes reside in the Golgi apparatus, where they probably form synthesising complexes along with other enzymes involved in the methylation of glucuronate side chains and acetylation of the backbone. The

preformed xylan is deposited in the cell wall, where it associates with cellulose microfibrils by hydrogen bonding (Kabel *et al.*, 2007; Busse-Wicher *et al.*, 2014) and may traverse several wall layers or be modified *in muro,* resulting in xylan epitope accumulation in the outer wall layers (Awano *et al.*, 2002). Different types of xylan-acting enzymes are known to reside in plant cell walls: endo-1,4-β-xylanase (EC 3.2.1.8), xylan endotransglycosylase (also known as trans-β-xylanase), 1,4-β-xylosidase (EC 3.2.1.37) and bifunctional α-arabinofuranosidase/β-xylosidase (Goujon *et al.*, 2003; Fry, 2004; Minic & Jouanin, 2006; Ichinose *et al.*, 2010; Franková & Fry, 2011; 2013; Johnston *et al.*, 2013).

Plant endo-1,4-β-xylanases belong to the glycoside hydrolase family 10 (GH10) and appear to be involved in xylan modification in primary and secondary walls, but their function is only understood for tissues undergoing decomposition involving digestion of cell wall xylan (Paull & Chen, 1983; Benjavongkulchai & Spencer, 1986; Slade *et al.*, 1989; Banik *et al.*, 1996; Cleemput *et al.*, 1997a, b; Bih *et al.*, 1999; Wu *et al.*, 2002; Simpson *et al.*, 2003; Chen & Paull, 2003; Suen & Huang, 2006). GH10 enzymes are also known to be highly expressed in xylem, but their function in this tissue is not yet clear (Mellerowicz *et al.*, 2001; Suzuki *et al.*, 2002; Geisler-Lee *et al.*, 2006). One of these genes, *PtxtXyn10A*, which shows high similarity to *AtXyn1* (Suzuki *et al.*, 2002), has been found to be upregulated during xylem secondary cell wall formation in hybrid aspen (*Populus tremula* L. x *tremuloides* Michx.) (Hertzberg *et al.*, 2001; Aspeborg *et al.*, 2005). Therefore, to investigate its function during xylogenesis, we analysed its activity, expression and effects of its suppression in hybrid aspen. We found that *PtxtXyn10A* acts mainly as a xylan endotransglycosylase and affects the cellulose microfibril angle (MFA) and other aspects of plant development. Based on our data, we propose that the main function of Xyn10A in secondary walls is to release mechanical stress arising during cell wall deposition.

Materials and Methods

Cloning of full length PtxtXyn10A

A partial clone of *PtxtXyn10A* was identified among the EST clones from a cambial region cDNA library of hybrid aspen (Sterky *et al.*, 2004). 5' RACE was carried out and full-length clones were obtained, cloned into the pGEM-T Easy vector (Promega, USA) and sequenced. The cDNA GenBank accession number is AY935501.

Plant material and growth conditions

Hybrid aspen, *Populus tremula* L. x *tremuloides* Michx., trees (clone T89) were grown in a greenhouse with a long photoperiod as described previously (Gray-Mitsumune *et al.*, 2008) until they reached approximately 2 m in height.

RT-qPCR analysis

One µg of total DNA-free RNA isolated from the primary- and secondary-walled developing xylem or transformed *A. thaliana* protoplasts was used for reverse transcription using an iScriptTM cDNA biosynthesis kit (Bio-Rad). Primers (Table S5) were designed using QuantPrime (http://www.quantprime.de) and Primer3Web 0.4.0 (http://primer3.sourceforge.net). The best reference gene (CYP in aspen and EF1a and UBQ5 in *Arabidopsis*) was selected using GeNorm (http://www.bigazelle.com; Vandesompele *et al.*, 2002) among ADF6, actin, UBQ CYP, EiF1a, clatrin and APT. An iQ^{TM} SYBR Green Supermix (BioRad) kit was used and Cq values were acquired using a Light Cycler 480 1.5.0.sp3 (Roche). Relative expression was calculated as $E_T{}^{(Cq1-Cq2)}/E_R{}^{(Cq1-Cq2)}$ in aspen (where E_T and E_R are the efficiencies of the target and reference genes, respectively, and Cq1 and Cq2 are the Cq levels for the sample and control, respectively) or as $2^{-\Delta\Delta Cq}$ (Livak *et al.*, 2001) in Arabidopsis.

Immunoblotting

For the production of polyclonal antibody Kamisa detecting *Ptxt*Xyn10A, a cDNA fragment from the clone A020P21 (accession number AI162606) encoding a C-terminal *Ptxt*Xyn10A fragment was cloned into pAFF8c-3c (Larsson *et al.*, 2000). The recombinant protein was produced in *E. coli* and purified using TALON® protein

purification columns (Clontech, USA). The purified 66 kDa soluble recombinant protein was used as antigen. For the production of antibody Abbe against the *Ptxt*Cel9B3 protein, a protein based on the full-length cDNA clone (accession number AY660968) was used in a similar fashion. The polyclonal antibodies were produced in rabbits by Agrisera AB, Sweden.

Soluble proteins were extracted according to Biswal *et al*. (2014), and cell wall bound proteins were extracted from the remaining pellet by incubation in Laemmli buffer (10% (v/v) glycerol, 5% (v/v) 2-mercaptoethanol, 2% (w/v) SDS, 62.5 mM Tris-HCl, pH 6.8) at 100°C for 10 min. The suspension was cooled to room temperature, subjected to centrifugation at 15000 g for 20 min, then 30 μg of each protein sample was loaded onto a NuPage® Novex Bis-Tris gel (Invitrogen, USA) and blotted onto a nitrocellulose membrane. The membrane was probed overnight at 4°C with a 1:1000 dilution of Kamisa antibody. Signals were revealed using the Amersham ECL System. The same membrane was subsequently probed with the antibody Abbe raised against a cell wall bound cellulase *Ptxt*Cel9B3 (Takahashi *et al.*, 2009).

Intracellular localization of* Ptxt*Xyn10A

PtxtXyn10A cDNA was subcloned into the binary vector pEarleyGate103 using the primers listed in Table S6. *Arabidopsis* was transformed using the floral dip method (Clough & Bent, 1998). Detection of recombinant protein was carried out as previously described (Latha Gandla *et al.*, 2014; Pawar PAM *et al.*, in revision).

Detection of endoxylanase and xylan endotransglycosylase activities in plants

Protein extraction. Secondary-walled developing xylem from transgenic and WT (T89) hybrid aspen was scraped and ground in liquid nitrogen. Soluble and wall-bound proteins were isolated as previously described (Biswal *et al*., 2014). All buffers contained complete protease inhibitor cocktail (Roche). Transfected *Arabidopsis* protoplats were harvested by centrifugation and proteins were extracted using buffer comprising 0.1 M Na succinate (pH=4.7) and 10 mM $CaCl_2$.

Thin-layer chromatography for detecting products of xylanase and xylan endotransglycosylase activities. Protein extracts containing either 1.25 mM or 6.25 mM

191 $Xylo_6$ (Megazyme, Ireland) were incubated at 40°C for 48 h. Volumes corresponding to
192 the same amounts of substrates were analysed on TLC Silica Gel 60 Glass plates as
193 described by Franková & Fry (2011).

194 ***Quantitative analysis of xylan endotransglycosylase using a fluorogenic substrate.*** To
195 prepare the fluorogenic substrate, 20 µg of $Xylo_6$ (Megazyme, Ireland) was labelled with
196 8-aminonaphthalene-1, 3, 6-trisulfonic acid (ANTS, Invitrogen) according to (Kosik *et al.*
197 (2012). The $NaCNBH_3$ was quenched with a two-fold molar excess of hydrochloric acid,
198 re-neutralised with NaOH to pH 7, dried in vacuum and re-dissolved in a small amount of
199 MilliQ water. The solution containing $Xylo_6$-ANTS was then spotted onto a dry column
200 packed with Silicagel 60 (Merck, Germany). The excess ANTS was washed out with *iso*-
201 propanol:NH_4OH:water (5:1:1, v/v/v) and 0.5 mL flow-through fractions were collected
202 and dried down. $Xylo_6$-ANTS was eluted off the column with 40% ethanol (v/v), dried
203 down in vacuum, reconstituted in a small amount of 3 M urea and electrophoresed on a
204 PACE gel together with the flow through fractions to ensure the purity of the product.
205 The concentration of $Xylo_6$-ANTS was estimated from absorbance measured at 365 nm
206 and calculated using a calibration curve.

207 An endotransglycosylation assay was performed according to Kosík *et al.* (2011) with the
208 following modifications: extracted proteins were incubated in 0.15% birch xylan (Sigma)
209 and 165 µM $Xylo_6$-ANTS at RT for 1 h. Reactions were loaded onto circles of Whatman
210 3MM chromatographic paper in ELISA UV plates, then washed and the bound
211 fluorescence measured using a Spectra Max Gemini (Molecular Devices) micro-plate
212 reader at 355 nm excitation and 538 nm emission. For the blank samples, reactions
213 without $Xylo_6$-ANTS were used. Product bound to 3MM paper was treated with 1 U of
214 either *endo*-1,4-beta-xylanase M1 from *T. viride* (Megazyme) or pectate lyase from *C.*
215 *japonicus* (Megazyme) used as an example of xylan-inert enzyme in extraction buffer or
216 in the extraction buffer only, for 1 h at 40°C. The reaction was stopped by washing three
217 times with 66% ethanol. Fluorescence of the remaining product was measured as above.

218 ***Xylanase activity.*** Azo-Xylan (from birchwood, Megazyme) was used for the
219 measurement of endoxylanase activity. The reaction was performed according to the
220 manufacturer's instructions for 20 h at 40°C in 0.1 M succinate buffer, pH 5.5. β-

xylanase M1 from *Trichoderma viride* (Megazyme) was used to construct the standard curve.

To quantify hydrolytic activity by reducing ends, 0.25% (w/v) birchwood xylan (Sigma) was incubated with extracted proteins in 0.1 M Na-succinate buffer, pH 5.5 at 40°C for 20 h. The reaction was stopped by boiling for 5 min in PAHBAH reagent (1.5% *p*-hydroxybenzoic acid hydrazide in 0.5 M NaOH) and absorbance was measured at 410 nm after cooling (Lever, 1972). Xylose (2 mM to 0.0078 mM) was used to construct the standard curve and the data were calibrated to units of β-xylanase M1 from *Trichoderma viride* (Megazyme).

Expression of* PtxtXyn10A *in Arabidopsis cells

Full length *PtxtXyn10A* cDNA was amplified (primers listed in Table S6). The products were cloned into the pENTR/D-TOPO vector (pENTR™ Directional TOPO® Cloning Kits, Invitrogen), sequenced and subsequently subcloned into the binary vector pK2WG7.0 (Karimi *et al.*, 2002) using the Gateway® system (Invitrogen).

An *Arabidopsis* cell suspension derived from roots was used for protoplast isolation and transient protoplast transformations according to Dóczi *et al.* (2011) with slight modifications: $5x10^5$ protoplasts were used for each transformation with 5 µg of plasmid DNA without any carrier. After transformation, protoplasts were incubated in the dark for 24 h and harvested by centrifugation at 300 *g* for 8 minutes.

Generation of transgenic antisense aspen

For the antisense construct, cDNAs of C-terminal fragments covering the whole catalytic module of *PtxtXyn10A* and 28 bp of the 3' end of CBM22_3$_{PtxtXyn10A}$ were amplified, cloned into the binary vector pPCV702.kana and transferred to hybrid aspen as described previously (Gray-Mitsumune *et al.*, 2008) using *Agrobacterium tumefaciens*.

FT-IR spectroscopic analysis

Wood at internode 44 from five to seven trees of selected lines and the WT were individually examined as previously described (Latha Gandla *et al.*, 2014). The initial PCA analysis was carried out with 28 observations and 624 variables on UV scaled pre-

249 treated spectra. After excluding outliers, OPLS-DA analyses (Trygg & Wold, 2002) were
250 performed to identify wavenumbers that distinguished different classes based on cell wall
251 composition. The OPLS-DA model was based on 21 observations and approximately 624
252 variables from Pareto-scaled pre-treated spectra using two classes (WT and transgenic).

253 ***Physicochemical wood analyses***

254 Transgenic antisense lines carrying the antisense *PtxtXyn10A* construct (lines 2, 3 and 32)
255 and a WT line (clone T89) were each represented by a minimum of 5 trees. Basal
256 internodes from trees approximately 2 m tall, taken below internode 46, were frozen in
257 liquid N and stored at -80°C. The samples were thawed, debarked, hand chipped and
258 dried before analysis.

259 ***Wet chemistry of wood.*** Bulk wood samples were analysed for lignin content and
260 carbohydrate composition as described in method AH 23-18 (Theander & Westerlund,
261 1986). The method involves full hydrolysis of samples, followed by derivatisation of
262 liberated monomers and gas chromatography. Lignin content (Klason and acid soluble)
263 was determined according to SCAN-C.1. The hemicellulose molecular weight was
264 determined using size-exclusion chromatography (SEC) according to Jacobs & Dahlman
265 (2001). Hemicellulose was isolated by extraction using 24% w/v KOH after
266 delignification of samples using chlorite and fractionated using hydrogel columns (120,
267 250, 500). An alkaline solution containing 0.2 M NaOH and 0.1 M acetate was used as
268 eluent. The molecular weight was calculated based on standard curves obtained from
269 fractionation and MALDI-TOF measurements (Jacobs & Dahlman, 2001).

270 The glucuronoxylan branching pattern was determined by PACE using
271 glucuronoxylanase GH30 as described in Bromley *et al.* (2013). Briefly, wood powder
272 was treated with 4 M NaOH, then neutralized with HCl, buffered with 0.1 M ammonium
273 acetate pH 6.0 and digested with glucuronoxylanase (*Bo*GH30; Bacova_03432,
274 Rogowski *et al.*, 2014) for 2 h at room temperature. Digestion products, along with no
275 enzyme and enzyme only controls, were labelled with ANTS, separated by
276 polyacrylamide gel electrophoresis as described in Goubet *et al*. (2002) and visualised
277 with a G-box UV gel documentation system (Syngene).

X-ray diffraction. Aspen stem segments without bark and pith were divided into three classes according to xylem thickness. Four replicates from the WT and three replicates from each of the transgenic antisense lines were measured in each size class after drying at 300 K. The X-ray diffraction experiments and data analysis for the determination of cellulose crystallite size, microfibril angle distribution and crystallinity index were conducted using CuKα_1 radiation (1.54 Å) as explained in Svedström *et al*. (2012).

Slit pit angle

Wood from internodes 42-43 was macerated as previously described (Gray-Mitsumune *et al.*, 2008). Cells were examined under an Axioplan 2 microscope (Zeiss). To measure the cellulose microfibril angle, the angle of slit pits was measured in three to five pits for each fibre, and at least 50 fibres were measured for each of three randomly selected trees per line.

Field-emission scanning electron microscopy

FAA-fixed stem segments from internode 30 were washed with water and sectioned to small cubes with a cryomicrotome (Microm HM 505E), treated with 0.1% (v/v) sodium hypochlorite for three min and dehydrated in an ethanol series prior to critical point drying. The specimens were mounted on an aluminium stub and coated with 5 nm iridium. For imaging, a Zeiss Merlin field emission SEM was used with 4 kV accelerating voltage.

Microarray analysis

RNA and array preparation was carried out according to UPSC-BASE standardized procedures (Sjödin *et al.*, 2006). The different scan levels for each slide were merged using restricted linear scaling (RLS) followed by step-wise normalization before further analysis. B-statistics were calculated against line 2 and 32 and the two lists of array elements were compared. Genes in antisense lines were considered differentially regulated if $B \geq 0$ and $P \leq 0.05$ compared to a reference WT. Genes selected from the ranking list of B-statistics were annotated against the *Populus* genome (Phytozome 9.0).

Statistical analysis

Univariate data were subjected to analysis of variance followed by post-hoc tests as indicated using the JMP 7 program (SAS Inc., USA). Multivariate data analysis was performed using SIMCA-P software (version 11.0.0.0, Umetrics AB, Sweden).

Results

Molecular cloning and bioinformatic analysis of PtxtXyn10A

The full-length *PtxtXyn10A* cDNA sequence was cloned from a cDNA library of developing xylem in hybrid aspen (GenBank accession number AY935501). The predicted *Ptxt*Xyn10A peptide lacks a signal sequence and contains three carbohydrate-binding modules family 22 (CBM22) followed by a Xyn10 catalytic domain (Fig. 1a). Five *N*-glycosylation sites and one processing site after R-329, releasing the mature peptide with molecular weight 65.3 kDa and pI = 5.77, were predicted by the sequence analysis.

Populus GH10 gene family

The *Populus trichocarpa* genome contains eight GH10 genes, *i.e. PtXyn10A* - *PtXyn10H*, of which seven have been previously identified (Geisler-Lee *et al.*, 2006) and one, *PtXyn10H*, was found in the region directly upstream of *PtXyn10A* on chromosome 2 (Fig. S1; Table S1). *PtXyn10A* and *PtXyn10H* have been merged into one model in the current version of Phytozome (9.1), but our rapid amplification of cDNA ends (RACE) and polymerase chain reaction (PCR) experiments confirmed the existence of two loci (Fig. S1; Table S1).

PtXyn10B lacks part of the catalytic domain and a corresponding truncated gene is also found in *Arabidopsis thaliana*. Phylogenetic analysis of the remaining genes of *P. trichocarpa* and *A. thaliana* (Henrissat *et al.*, 2001) has revealed four well-defined clades with members in both species (Fig. S2). The clade to which *PtXyn10A* belongs, together with its closest paralog *PtXyn10H* and four Arabidopsis genes, including *AtXyn1*, is characterised by the presence of 2-4 CBMs. Other clades include genes with one CBM or none.

Xyn10A ***is the main GH10 transcript in secondary-walled developing xylem***

Reverse transcription-PCR (RT-PCR) revealed a high abundance of *PtxtXyn10A* transcripts in stems and roots with secondary growth and low abundance in the apical bud and mature leaves (Fig. S3a), consistent with its localisation to developing secondary-walled xylem seen in microarray studies (Hertzberg *et al.*, 2001; Aspeborg *et al.*, 2005).

To determine in which xylem cell types *PtxtXyn10A* is expressed, we performed *in situ* RT-PCR in stem sections using gene-specific nested primers (Gray-Mitsumune *et al.*, 2004). *Xyn10A*-specific signals were detected in all cell types in developing wood, fibres, vessel elements and ray cells, with the highest expression observed during the early stages of secondary wall deposition (Fig. S3b).

To compare the expression pattern of *Xyn10A* in wood-forming tissues to that of other *Populus* GH10 family members, we examined the relative transcript abundance of GH10 genes in cambium/phloem versus secondary wall developing xylem by RT-qPCR. Transcripts of *Xyn10A, Xyn10D, Xyn10E* and *Xyn10G* were detected in developing xylem, but only *Xyn10A* was highly upregulated in the secondary wall forming xylem (Fig. S4a). Moreover, based on *Populus* microarray data (http://bar.utoronto.ca/; Wilkins *et al.*, 2009), the expression levels of other GH10 genes were found to be several orders of magnitude lower than those of *Xyn10A* in developing wood (Fig. S4b).

Xyn10A protein is present in xylem cell walls **as a** ***68 kDa peptide***

To detect the Xyn10A protein in wood-forming tissues, the polyclonal antibody named "Kamisa" was raised against the C-terminal part of the *Ptxt*Xyn10A peptide. Soluble proteins were removed from crude plant extracts using a low ionic strength buffer, and proteins bound to the remaining pellet, including cell wall bound proteins, were extracted with a sodium dodecyl sulphate (SDS) containing buffer. A clear band at approximately 68 kDa was detected in the cell wall fraction from developing xylem consistent with the expected processed 65 kDa protein together with predicted glycosylations (Fig. 1b). No signal was detected in the soluble fraction from this tissue or in any fraction from the apical bud tissues in which the gene was lowly expressed (Fig. S3a).

Although *Ptxt*Xyn10A lacks a predicted signal peptide (Table S1), the SecretomeP 2.0 server (http://www.cbs.dtu.dk/services/SecretomeP/) predicted its target to be the apoplasm. To verify the cellular localization experimentally, a 35S::*Ptxt*Xyn10A:eGFP construct was expressed in Arabidopsis. The GFP signal was detected in cell walls, but it was weak and labile, probably due to the acidic pH of cell walls. However, the fusion protein was clearly immunolocalised in cell walls after protoplast plasmolysis (Fig. 1c).

Aspen xylem wall-bound proteins exhibit xylan endotransglycosylase and xylanase activities in a substrate concentration-dependent manner

Both xylanase and xylan endotransglycosylase activities have been detected in plant tissues, latter activity requiring higher substrate concentration (Franková & Fry, 2011; Johnston *et al.*, 2013). A similar dependence of activity on substrate concentration is also known for microbial GH10 enzymes (Charnock *et al.*, 1997). Therefore, we investigated if such activities could be detected in proteins extracted with high ionic strength buffer from developing xylem (where *Ptxt*Xyn10A is expressed as the main GH10 enzyme) when using xylohexaose as substrate. Under these conditions, it was expected that hydrolytic activity would yield products with DP 1-5, whereas endotransglycosylase activity would give a mixture of products with larger and lower DP than 6. When 1.85 mM xylohexaose was incubated with aspen protein extracts, products with DP 1 to DP 5 accumulated in a time-dependent manner, indicative of hydrolysis (Fig. 2a). However, when the concentration of xylohexaose was increased to 4 mM (data not shown) or 6.125 mM, products with DP values ranging from 8 to 10 were additionally detected, indicative of endotransglycosylation (Fig. 2a). The main products had DP 9 and DP 3, corresponding to cleavage in the middle of xylohexaose followed by transglycosylation. This shows that developing xylem cells exhibit xylan hydrolase and xylan endotransglycosylase activities and that the endotransglycosylase activity requires a higher substrate concentration than hydrolase (> 1.85 mM xylohexaose in the present experimental setup).

To establish a quantitative assay for xylan endotransglycosylation in high ionic strength protein extracts of developing wood, the extracts were incubated with birchwood xylan

(the donor) and 8-aminonaphtalene-1,3,6-trisulfonic acid-labelled Xylo6 (Xylo6-ANTS; the acceptor). Xylan endotransglycosylation resulted in a high molecular weight ANTS labelled product, which was bound to cellulose and detected by fluorimetry (Fig. 2b). This product was significantly more susceptible to xylanase M1 than to pectate lyase or reaction buffer, confirming that it was xylan-labelled with ANTS (Fig. 2c). Decreased fluorescence observed after incubation in the buffer at 40°C was attributed to the instability of ANTS.

Ptxt*Xyn10A expression in* Arabidopsis *cells strongly increases xylan endotransglycosylation but not xylan hydrolysis*

To investigate which activity (xylan hydrolase or xylan endotransglycosylase) was encoded by *PtxtXyn10A*, *Arabidopsis* protoplasts were transfected by either *Ptxt*Xyn10A or an empty vector and proteins were extracted from the samples expressing the transgenes, as verified by RT-qPCR. Xylan endotransglycosylation detected by ANTS assay was significantly increased in cells expressing *Ptxt*Xyn10A compared to the empty vector control (Fig. 3a).

The same samples were tested for xylanase activity using either the *endo*-1,4-*ß*-xylanase assay measuring solubilisation of AZO-xylan or the reducing end assay. Weak xylanase activity (four orders of magnitude lower than that of M1 xylanase from *Trichoderma viride* used for normalisation) was detected by these two assays in extracts for the empty vector and *PtxtXyn10A* expressing cells, and no significant differences between these extracts were detected (Fig. 3b and c). These results indicate that *PtxtXyn10A*-encoded enzyme exhibits xylan endotransglycosylase rather than xylanase activity *in vitro*.

Suppression of PtxtXyn10A *expression in transgenic aspen*

To study the physiological role of *Ptxt*Xyn10A, ten transgenic antisense lines of hybrid aspen were generated and two or three most highly affected antisense lines were selected for subsequent analyses. *Ptxt*Xyn10A transcript levels were decreased to approx. 50% of the WT level in the selected lines (Fig. 4a) and western blotting using Kamisa antibody showed a corresponding reduction of *Ptxt*Xyn10A protein in extracts obtained from xylem with high ionic strength buffer (Fig. 4b). The xylan endotransglycosylation by

these extracts was significantly lower in transgenic antisense lines compared to WT (Fig. 4c), but the xylanase activity was not affected (Fig. 4 d). These data indicate that the suppression of *PtxtXyn10A* affects xylan endotransglycosylase but not xylanase activity in developing wood.

The transgenic antisense lines exhibited increased growth in height, internode number and leaf size (Fig. 5). Stem diameters and petiole lengths were also recorded, but no clear changes were detected for these variables. To investigate if the increased growth was caused by a change in the primary cell wall plasticity, thereby affecting cell size, casts were prepared from the adaxial leaf epidermis and the cell surface area was determined by microscopy. No significant difference in cell surface area between the transgenic antisense lines and WT was found (Fig. 5). Thus, *PtxtXyn10A* suppression does not increase leaf growth by increasing primary wall plasticity but by stimulating cell division.

Effects of PtxtXyn10A on xylan structure

The two putative activities of *Ptxt*Xyn10A were expected to differentially affect xylan chain length: xylanase would decrease it, whereas xylan endotransglycosylase may increase, decrease or not affect it depending on the length of input acceptor; without any input, the average length of xylan should not be altered by endotransglycosylation. Size exclusion chromatography of a 24% (w/v) KOH-extracted hemicellulose fraction containing mainly glucuronoxylan (Jacobs & Dahlman, 2001) gave similar weight-averaged molecular weights (M_w) for WT (15 600) and transgenic antisense lines (15 100 to 15 500); the polydispersivity index (M_w/M_n) ranged between 1.13 and 1.14 for all the lines (Table S2). Thus, no major change in glucuronoxylan molecular weight was detected, consistent with *Ptxt*Xyn10A acting as an endotransglycosylase *in vivo*.

To determine if the (Me)GlcA branching pattern of glucuronoxylan was affected by the endotransglycosylase activity, we used glucuronoxylanase *Bo*GH30, which acts specifically on the xylan backbone and cleaves only when it is substituted with (Me)GlcA at the –2 position. The lengths of the digestion products thus corresponded to intervals of (Me)GlcA substitutions on the xylan backbone. PACE analysis of the labelled digestion products gave similar profiles for the transgenic antisense lines and WT aspen (Fig. 6).

The detected bands agreed with those previously described in *Arabidopsis* xylan (Bromley *et al*., 2013) and corresponded to oligosaccharides arising from two xylan domains: evenly spaced longer (DP 6 to DP over 20) oligosaccharides of the major domain and shorter (DP 5 to 7), odd or even length fragments derived from the minor domain. The presence of both types of products in all examined lines indicates that both xylan domains are present in aspen wood and are not affected by the xylan endotransglycosylase activity.

Effects of* PtxtXyn10A *on wood cell wall composition

To determine whether reduced xylan endotransglycosylase activity affects other polymers in cell wall, diffuse reflectance Fourier-transformed infrared (FT-IR) spectra of milled wood of transgenic and WT plants were analysed. Orthogonal projections to latent structure discriminant analysis (OPLS-DA) showed separation of the transgenic and WT spectra, indicating alterations in cell wall composition (Fig. 7 a). Among the bands contributing to the separation, there were several vibrations corresponding to different forms of lignin. The 1460 cm^{-1} band (C-H deformation/bending in aromatics; Dokken *et al.*, 2005) and 1506/1595 band ratio, which reflects the condensed and cross-linked lignin structure (Akin *et al.*, 1993; Stewart *et al.*, 1997), were increased in the transgenic lines (Fig. 7 b). The ratio of absorbance at 1506 cm^{-1} to that at 900 cm^{-1} (representing the anomeric C-O stretch in cellulose (Zhong *et al.*, 2000)) was significantly higher in the transgenic lines, suggesting that they may have more lignin relative to cellulose. The observation that the entire spectral region between 1000–1100 cm^{-1} (sugar-ring vibrations) was more intense in the WT also indicates a higher lignin to cellulose ratio in the transgenic lines as the corresponding carbohydrates were less likely to be hemicelluloses or pectins because their intensity negatively correlated with that of the 1730 cm^{-1} –C=O vibration (Fig. 7 b).

To support these conclusions, we performed wet chemical analyses on wood material from the transgenic lines and WT. These analyses showed that the content of galactose and glucose was decreased, whereas the content of xylose and lignin was increased in the transgenic lines compared to WT (Table 1). Thus, the analysis confirmed the increased

lignin to cellulose ratio in the transgenic lines seen by FT-IR and additionally revealed increased xylan and reduced galactan content. Low xylan and high galactan contents are diagnostic for gelatinous fibres found in tension wood in aspen (Mellerowicz & Gorshkova, 2012), and therefore the observed changes in cell wall monosaccharide composition suggest a decreased tension wood content in the stems of transgenic lines as compared to WT.

Effects of altered PtxtXyn10A *expression on cell wall architecture*

Based on the results for *PtxtXyn10A* expression (Figs S4; Aspeborg *et al.*, 2005; Andersson-Gunneråas *et al.*, 2006; Winzéll *et al.*, 2010), we anticipated its involvement during secondary cell wall formation. Therefore, wood cross sections were analysed in transgenic and WT plants by light and transmission electron microscopy (Fig. S5). However, no major changes were detected. Light microscopy of isolated wood cells revealed a small reduction in fibre diameter and length and a corresponding small increase in wood density (Fig. S6). We also noted a significant change in the slit pit angles in the fibres (Fig. 8a). Since the slit pit orientation corresponds to the cellulose microfibril orientation in the S2 layer (Donaldson, 2008), we tested whether the reduced endotransglycosylase activity affected the cellulose microfibril angle (MFA) in the transgenic lines by performing X-ray diffraction analysis of the transgenic and WT wood samples. To remove the potential effects of variable tension wood content in these samples, the cellulose crystallite width was used to identify samples containing tension wood. Whereas the majority of WT and transgenic antisense samples had an average crystallite width between 29 and 31 Å, within the range typically reported for *Populus* wood (Yamamoto *et al.*, 2010; Leppänen *et al.*, 2011), approximately one third of the samples exhibited crystallite widths greater than 31 Å, typical for tension wood (reviewed by Mellerowicz & Gorshkova, 2012). These samples were set aside as tension wood enriched samples. Cellulose MFA in the remaining normal wood samples was clearly reduced in the transgenic antisense lines (Fig. 8b), indicating that Xyn10A activity is needed to orient cellulose microfibrils at large angles to the fibre axis in secondary walls.

To investigate if the morphology of cellulose microfibrils was also affected, the topology

of cell walls was visualized by field emission scanning electron microscopy (FE-SEM). The images revealed an ordered, strictly parallel, dense array of microfibrils in the S2 layer in all genotypes (Fig. 8c). The microfibrils had a "Z" orientation, similar to the pattern previously reported for conifers (Abe *et al.*, 1992). No major change in microfibril topology was observed in the transgenic antisense line, except for a more axial microfibril orientation as compared to WT.

Analysis of global gene expression pattern in transgenic antisense plants

To investigate the effects of reduced *PtxtXyn10A* expression on the transcriptome, the global transcript profiles of developing xylem stem tissues of lines 2, 32 and WT were analysed using a 25K *Populus* (POP2) microarray (Sterky *et al.*, 2004). 123 genes were affected ($P \leq 0.05$ and $B \geq 0$) in both antisense lines, of which 76 were downregulated (Tables S3 and S4). More genes were significantly affected in line 2 than 32, in agreement with the stronger *PtxtXyn10A* suppression in this line. 61 of the affected genes could be assigned functional categories, which included signal transduction, carbohydrate metabolism and cell wall, transcription and translation, energy, cell division and cellular transport. Among the signal transduction related transcripts, several stress perception and ethylene-signalling transcripts were affected, including ones possibly involved in mechano-perception (leucine-rich receptor-like kinases, Ca-signalling related proteins, microtubule-associated proteins), which were upregulated (Table 2). Within the cell wall related category, the most striking change was the downregulation of cellulose biosynthesis related genes, including *COBRA-LIKE 4*, *FRUCTOKINASE* and *CEL9A1 (Populus* ortholog of *KORRIGAN1*), and fasciclin-like arabinogalactan proteins, which are the markers of tension wood formation (Lafarguette *et al.*, 2004; Andersson-Gunnerås *et al.*, 2006). In contrast, the expression of *PHENYLALANINE AMMONIA-LYASE* (*PAL1*) responsible for the first step of the lignin biosynthetic pathway was increased (Table 2). Over 60% of the genes downregulated in transgenic antisense lines (Table S2) were upregulated during the tension wood response (Andersson-Gunnerås *et al.*, 2006), strongly indicating that downregulation of *PtxtXyn10A* affects the tension wood and stress responses and that tension wood formation was inhibited in the transgenic antisense lines.

Discussion

PtxtXyn10A *encodes a xylan endotransglycosylase*

GH10 xylanases follow a retaining catalytic mechanism similar to that of xyloglucan endotransglucosylases (Henrissat *et al.*, 2001), which allows both xylanase and xylan endotransglycosylase activities. In plants, xylanase activity of GH10 enzymes was demonstrated in cereals during caryopsis germination and pollen development (Bih *et al.*, 1999; Caspers *et al.*, 2001; Wu *et al.*, 2002). Recently, several vascular plants were shown to have extractable xylanase and xylan endotransglycosylase activities, the latter activity increasing at high 1,4-β-xylo-oligosaccharide concentration (Franková & Fry, 2011; Johnston *et al.*, 2013). Here, we have shown that these activities are also present in developing wood of aspen (Fig. 2). Four lines of evidence indicate that *Ptxt*Xyn10A is responsible for the observed xylan endotransglycosylase activity in developing wood. First, *Ptxt*Xyn10A is the main GH10 enzyme expressed in this tissue (Fig. S 4). Second, the heterologous expression of *Ptxt*Xyn10A in *Arabidopsis* protoplasts increased xylan endotransglycosylase, whereas xylanase activity was not affected (Fig. 3). Third, the downregulation of *PtxtXyn10A* in hybrid aspen suppressed xylan endotransglycosylase activity without affecting xylanase activity (Fig. 4). Fourth, the suppression of *Ptxt*Xyn10A activity in hybrid aspen did not result in an increased glucuronoxylan molecular weight as would be expected if it were an endoxylanase (Table S2).

PtxtXyn10A undergoes proteolytic processing and is transported to the apoplasm via a non-classical pathway

The size of the *Ptxt*Xyn10A protein detected in the cell wall bound protein fraction provides clues to its processing, which according to the predicted cleavage site would leave CBM22_3 and the catalytic domain in the mature protein (Fig. 1). The role of the processing is presently unclear, but it does not seem to be a limiting step in the protein biosynthesis as we never observed the full-length peptide even after overexpressing the full length cDNA (data not shown), indicating that the processing step must be very rapid. Several plant xylanases have been reported to undergo proteolytic processing, and in those cases, a single CBM22 and sometimes an additional short peptide at the C-

terminal end are removed (Caspers *et al.*, 2001; Wu *et al.*, 2002; Chen & Paull, 2003; Van Campenhout *et al.*, 2007; De Backer *et al.*, 2010). Processing has been suggested to increase xylanase activity and facilitate secretion to the apoplasm (Caspers *et al.*, 2001; De Backer *et al.*, 2010), but the responsible protease and mechanism of transport facilitation are still unknown.

All known plant GH10 enzymes are active in the cell wall and mechanisms of their transport to this compartment vary. Aleurone layer and tapetum xylanases accumulate in cytoplasm and are released to endosperm or developing pollen grains, respectively, following programmed cell death and disintegration of their source cells (Bih *et al.*, 1999; Caspers *et al.*, 2001). In contrast, papaya *Cpa*EXY1 is secreted via the classical ER-Golgi route with participation of the signal peptide (Chen & Paull, 2003). Although both *Ptxt*Xyn10A and its orthologue *At*Xyn1 lack the predicted signal peptide, they accumulate in the cell wall (Fig. 1; Suzuki *et al.*, 2002) after being transported via a non-classical pathway (Agrawal *et al.*, 2010).

Suppression of PtxtXyn10 activity stimulates primary growth

The stimulatory effects of *PtxtXyn10A* suppression on stem elongation, leaf expansion and the number of internodes observed in this study are intriguing (Fig. 5). The lack of accompanying cell size increase as found for leaf epidermis and xylem cells strongly indicates that these effects are not mediated by primary wall plasticity but rather related to metabolism of xylan in secondary walls. The observed growth stimulation could be mediated by mechanical or oligosaccharide signalling. It is also possible that the suppression of xylan endotransglycosylase activity in spirally thickened protoxylem elements changes their mechanical properties, such that they are more easily stretched during organ growth, which in turn most likely leads to increased primary organ expansion (Paolillo & Rubin, 1991).

Ptxt*Xyn10 activity regulates MFA in secondary walls, probably by affecting mechano-perception*

PtxtXyn10A is co-regulated with xylan biosynthesis genes during secondary wall formation (Mellerowicz & Sundberg, 2008) and induced by *Pt*MYB021, the transcription

596 factor responsible for secondary wall initiation (Winzéll *et al.*, 2010). It is also strongly
597 downregulated during tension wood formation (Andersson-Gunnerås *et al.*, 2006). These
598 expression patterns indicate that the encoded xylan endotransglycosylase plays a specific
599 role during secondary wall biosynthesis.

600 Our results show that although *Ptxt*Xyn10A activity neither affects xylan chain length
601 (Table S2) nor its branching pattern (Fig. 6), its suppression affects many aspects of plant
602 development, *i.e.* cellulose orientation in secondary walls (Fig. 8), tension wood
603 formation (Tables 1 & 2) and plant primary growth (Fig. 5). We propose that analogous
604 to xyloglucan endotransglucosylase activity, which releases tension in primary cell wall
605 during growth, xylan endotransglycosylase activity may release tension in secondary
606 walls. Such tension is envisaged to arise during self-assembly of the cellulose-xylan
607 network, during which cellulose microfibrils are deposited along rigid cortical
608 microtubules that orient the cellulose network (Baskin, 2001; Gardiner *et al.*, 2003;
609 Funada, 2008; Li *et al.*, 2012) and are immediately coated by negatively charged
610 glucuronoxylan (Stevanic & Salmén, 2009). It has been suggested that the
611 glucuronoxylan coat on the surface of cellulose microfibrils creates repulsive electrostatic
612 forces (Reis & Vian, 2004). The fact that such repulsive forces operate in cell wall can be
613 deduced from the behaviour of negatively charged cellulose crystals in solution; at high
614 concentrations, the cellulose fibrils arrange spontaneously in regular patterns forming
615 liquid crystals (Reis *et al.*, 1991; Lagerwall *et al.*, 2014). Another source of tension
616 stresses is the cross linking of microfibrils by xylan.

617 If the role of *Ptxt*Xyn10A is to relieve such growth stresses, its suppression would result
618 in excessive build-up of stresses that would trigger mechano-perception reactions.
619 Although very little is known about mechano-perception in plants, the emerging picture
620 points towards cortical microtubules as effectors of tensional stress signals (Jacques *et*
621 *al.*, 2013; Landrein & Hamant, 2013). Cortical microtubules assume either a random or
622 parallel orientation under control of Katanin and SPIRAL2 (Wightman *et al.*, 2013), and
623 can reorient within hours following different stimuli (Lindeboom *et al.*, 2013), resulting
624 in a change in MFA. Thus, we suggest that *Ptxt*Xyn10A suppression may trigger
625 mechano-perception, which in turn re-orients cortical microtubules, resulting in the
626 reduction of MFA (Fig. 9).

Since tension wood induction is thought to involve mechano-perception, another prediction that follows from our hypothesis is that the suppression of xylan endotransglycosylase activity may interfere with the tension wood response. The observed effects in aspen (Tables 1 & 2) are compatible with this hypothesis.

Other factors affecting cell wall self-assembly, for example pectin metabolism (Yoneda *et al.*, 2010) or fasciclin-domain arabinogalactan proteins FLA11 and FLA12 (MacMillan *et al.*, 2010), are believed to influence the orientation of cellulose microfibrils. Several authors have suggested that glucuronoxylan plays a role in determining MFA (Reis & Vian, 2004; Ruel *et al.*, 2006). Its abundance and MFA in different secondary wall layers were shown to be correlated in radiata pine (Donaldson & Knox, 2012). Moreover, in white spruce, the *Xyn10* locus was found to be associated with MFA (Beaulieu *et al.*, 2011). Here, we have provided empirical evidence that *PtxtXyn10A* affects MFA in wood fibres in hybrid aspen and proposed a mechanism for such regulation.

Acknowledgements

We thank Kjell Olofsson, Andreas Sjödin and Oskar Skogström, Laszlo Bako, Kirsi Leppänen and Gaia Geiss for help with the anatomy, microarrays, protoplasts, X-ray and qPCR analyses, respectively, and Anne Gouget, Lorenz Gerber and Tarek Elhasi for preliminary experiments. András Gorzsás from the Vibrational Spectroscopy Platform at Umeå University assisted with the FTIR spectroscopic analysis and Cheng Choo Lee at the Umeå Electron Microscopy Core Facility with FE-SEM.

Literature Cited

Abe H, Ohtani J, Fukazawa K. 1992. Microfibrillar orientation of the innermost surface of conifer tracheid wall. *IAWA Bulletin* **13**: 411–417.

Agrawal GK, Jwa NS, Lebrun MH, Job D, Rakwal R. 2010. Plant secretome: Unlocking secrets of the secreted proteins. *Proteomics* **10**: 799–827.

Akin E, Himmelsbach DS, Carl RT, Hanna WW, Barton FE II. 1993. Mid-infrared

655 microspectroscopy to assess lignin in plant tissues related to digestibility. *Agronomy*
656 *Journal* **85**: 171–175.

657 **Andersson-Gunneråas S, Mellerowicz EJ, Love J, Segerman B, Ohmiya Y, Coutinho**
658 **PM, Nilsson P,Henrissat B, Moritz T, Sundberg B. 2006.** Biosynthesis of cellulose-
659 enriched tension wood in *Populus*: global analysis of transcription and metabolites
660 identifies biochemical and developmental regulators in secondary wall biosynthesis.
661 *Plant Journal* **45**: 144–165.

662 **Aspeborg H, Schrader J, Coutinho PM, Stam M, Kallas Å, Djerbi S, Nilsson P,**
663 **Denman S, Amini B, Sterky F *et al*. 2005.** Carbohydrate-active enzymes involved in the
664 secondary cell wall biogenesis in hybrid aspen. *Plant Physiology* **137**: 983–997.

665 **Awano T, Takabe K, Fujita M. 2002.** Xylan deposition on secondary wall of *Fagus*
666 *crenata* fiber. *Protoplasma* **219**: 106–115.

667 **Banik M, Garrett TPJ, Fincher GB. 1996.** Molecular cloning of cDNAs encoding (14)-
668 β-xylan endohydrolases from the aleurone layer of germinated barley (*Hordeum*
669 *vulgare*). *Plant Molecular Biology* **31**: 1163–1172.

670 **Baskin TI. 2001.** On the alignment of cellulose microfibrils by cortical microtubules: a
671 review and a model. *Protoplasma* **215**: 150–171.

672 **Beaulieu J, Doerksen T, Boyle B, Clément S, Deslauriers M, Beauseigle S, Blais S,**
673 **Poulin PL, Lenz P, Caron S *et al*. 2011.** Association genetics of wood physical traits in
674 the conifer white spruce and relationships with gene expression. *Genetics* **188:** 197–214.

675 **Benjavongkulchai E, Spencer MS. 1986.** Purification and characterization of barley-
676 aleurone xylanase. *Planta* **169**: 415–419.

677 **Bevan MW, Franssen MCR. 2006.** Investing in green and white biotech. *Nature*
678 *Biotechnology* **24**: 765–767.

679 **Bih FY, Wu SS, Ratnayake C, Walling LL, Nothnagel EA, Huang AH. 1999.** The
680 predominant protein on the surface of maize pollen is an endoxylanase synthesized by a
681 tapetum mRNA with a long 5' leader. *Journal of Biological Chemistry* **274**: 22884–
682 22894.

683 **Biswal AK, Soeno K, Latha Gandla M, Immerzeel P, Pattathil S, Lucenius J,**
684 **Serimaa R, Hahn MG, Moritz T, Jönsson LJ, Israelsson-Nordström M, Mellerowicz**
685 **EJ**. **2014**. Aspen pectate lyase *PtxtPL1-27* mobilizes matrix polysaccharides from
686 woody tissues and improves saccharification yield. *Biotechnology for Biofuels* **7**:11.

687 **Busse-Wicher M, Gomes TCF, Tryfona T, Nikolovski N, Stott K, Grantham NJ,**
688 **Bolam DN, Skaf MS, Dupree P. 2014.** The pattern of xylan acetylation suggests xylan
689 may interact with cellulose microfibrils as a two-fold helical screw in the secondary plant
690 cell wall of *Arabidopsis thaliana. Plant Journal* in press.

691 **Bromley JR, Busse-Wicher M, Tryfona T, Mortimer JV, Zhang Z, Brown D,**
692 **Dupree P. 2013.** GUX1 and GUX2 glucuronyltransferases decorate distinct domains of
693 glucuronoxylan with different substitution patterns. *Plant Journal* **74**: 423–434.

694 **Brummell DA, Schröder R. 2009.** Xylan metabolism in primary cell walls. *New*
695 *Zealand Journal of Forestry Science* **39**: 125–143.

696 **Caspers MPM, Lok F,Sinjorgo KMC, van Zeijl MJ, Nielsen KA, Cameron-Mills V.**
697 **2001.** Synthesis, processing and export of cytoplasmic *endo*-beta-1,4-xylanase from
698 barley aleurone during germination. *Plant Journal* **26**:191–204.

699 **Charnock SJ, Lakey JH, Virden R, Hughes N, Sinnott ML, Hazelwood GP,**
700 **Pickergill R, Gilbert HJ. 1997.** Key residues in subsite f play a critical role in the
701 activity of *Pseudomonas fluorescens* subspecies *cellulosa* xylanase a against
702 xylooligosaccharides but not against highly polymeric substrates such as xylan. *Journal*
703 *of Biological Chemistry* **272**: 2942–2951.

704 **Chen NJ, Paull RE. 2003.** Endoxylanase expressed during papaya fruit ripening:
705 purification, cloning and characterization. *Functional Plant Biology* **30**: 433–441.

706 **Cleemput G, Hessing M, Van Oort M, Deconynck M, Delcour JA. 1997a.** Purification
707 and characterization of a beta-D-xylosidase and an endo-xylanase from wheatflour. *Plant*
708 *Physiology* **113**: 377–386.

709 **Cleemput G, Van Laere K, Hessing M, Van Leuven F, Torrekens S, Delcour JA.**
710 **1997b.** Identification and characterization of a novel arabinoxylanase from wheat flour.
711 *Plant Physiology* **115**: 1619–1627.

Clough SJ, Bent AF. 1998. Floral dip: a simplified method for *Agrobacterium*-mediated transformation of *Arabidopsis thaliana. Plant Journal* **16**: 735–743.

Darvill JE, Mcneil M, Darvill AG, Albersheim P. 1980. Structure of plant-cell walls. II. Glucuronoarabinoxylan, a 2nd hemicellulose in the primary-cell walls of suspension-cultured sycamore cells. *Plant Physiology* **66**: 1135–1139.

De Backer E, Gebruers K, Van den Ende W, Courtin CM, Delcour JA. **2010.** Post-translational processing of beta-d-xylanases and changes in extractability of arabinoxylans during wheat germination. *Plant Physiology* and *Biochemistry* **48**: 90–97.

Dóczi R, Hatzimasoura E, Bögre L. 2011. Mitogen-activated protein kinase activity and reporter gene assays in plants. *Methods* in *Molecular Biology* **779**: 79–92**.**

Dokken KM, Davis LC, Marinkovic NS. 2005. Use of infrared microspectroscopy in plant growth and development. *Applied Spectroscopy Reviews* **40:** 301–326.

Donaldson LA. (2008) Microfibril angle: measurement, variation and relationships – a review. *IAWA Journal* **29**: 345–386.

Donaldson LA, Knox JP. 2012. Localization of cell wall polysaccharides in normal and compression wood of radiata pine: relationships with lignification and microfibril orientation. *Plant Physiology* **158**: 642–653.

Ebringerová A, Heinze T. 2000. Xylan and xylan derivatives – biopolymers with valuable properties. Naturally occurring xylan structures, procedures and properties. *Macromolecular Rapid Communications* **21**: 542–556.

Franková L, Fry SC. 2011. Phylogenetic variation in glycosidases and glycanases acting on plant cell wall polysaccharides, and the detection of transglycosidase and trans-β-xylanase activities. *Plant Journal* **67**: 662–681.

Franková L, Fry SC. 2013. Biochemistry and physiological roles of enzymes that 'cut and paste' plant cell-wall polysaccharides. *Journal of Experimental Botany* **64**: 3519–3550.

Fry S. 2004. Primary cell wall metabolism: tracking the careers of wall polymers in living plant cells. *New Phytologist* **161**: 641–675.

Funada R. 2008. Microtubules and the control of wood formation. In: Nick P, editor. *Plant microtubules: development and flexibility*. Springer-Verlag, Berlin, pp 83–119.

Gardiner JC, Taylor NG, Turner SR. 2003. Control of cellulose synthase complex localization in developing xylem. *Plant Cell* **15**: 1740–1748.

Geisler-Lee J, Geisler M, Coutinho PM, Segerman B, Nishikubo N, Takahashi J, Aspeborg H, Djerbi S, Master E, Andersson-Gunneråas S *et al.* 2006. Poplar carbohydrate-active enzymes. Gene identification and expression analyses. *Plant Physiology* **140**: 946–962.

Goubet F, Jackson P, Deery MJ, Dupree P. 2002. Polysaccharide analysis using carbohydrate gel electrophoresis. A method to study plant cell wall polysaccharides and polysaccharide hydrolases. *Analytical Biochemistry* **300**: 53–68.

Goujon T, Minic Z, El Amrani A, Lerouxel O, Aletti E, Lapierre C, Joseleau JP, Jouanin L. 2003. *AtBXL1*, a novel higher plant (*Arabidopsis thaliana)* putative beta-xylosidase gene, is involved in secondary cell wall metabolism and plant development. *Plant Journal* **33**: 677–690.

Gray-Mitsumune M, Abe H, Takahashi J, Sundberg B, Mellerowicz EJ. 2004. Liquid phase fluorescence in situ RT-PCR analysis for gene expression analysis in woody stems. *Plant Biology* **6**: 47–54.

Gray-Mitsumune M, Blomquist K, McQueen-Mason S, Teeri TT, Sundberg B, Mellerowicz EJ. 2008. Ectopic expression of a wood-abundant expansin *PttEXPA1* promotes cell expansion in primary and secondary tissues in aspen. *Plant Biotechnology Journal* **6**: 62–72.

Henrissat B, Coutinho PM, Davies GJ. 2001. A census of carbohydrate-active enzymes in the genome of *Arabidopsis thaliana. Plant Molecular Biology* **47**: 55–72.

Hertzberg M, Aspeborg H, Schrader J, Andersson A, Erlandsson R, Blomqvist K, Bhalerao R, Uhlen M, Teeri TT, Lundeberg J *et al.* 2001. A transcriptional road map to wood formation. *Proceeding of the National Academy of Sciences of the United States of America* **98**: 14732–14737.

Ichinose H, Nishikubo N, Demura T, Kaneko S. 2010. Characterization of a-L-

arabinofuranosidase related to the secondary cell walls formation in *Arabidopsis thaliana*. *Plant Biotechnology* **27**: 259–266.

Imamura T, Watanabe T, Kuwahara M, Koshijima T. 1994. Ester linkages between lignin and glucuronic-acid in lignin-carbohydrate complexes from *Fagus crenata*. *Phytochemistry* **37**: 1165–1173.

Jacobs A, Dahlman O. 2001. Characterization of the molar masses of hemicelluloses from wood and pulps employing size exclusion chromatography and matrix-assisted laser desorption ionization time-of-flight mass spectrometry. *Biomacromolecules* **2**: 894–905.

Jacques E, Verbelen J-P, Vissenberg K. 2013. Mechanical stress in Arabidopsis leaves orients microtubules in a 'continuous' supracellular pattern. *BMC Plant Biology* **13**:163.

Johnston SL, Prakash R, Chen NJ, Kumagai MH, Turano HM, Cooney JM, Atkinson RG, Paull RE, Cheetamun R, Bacic A *et al.* 2013. An enzyme activity capable of endotransglycosylation of heteroxylan polysaccharides is present in plant primary cell walls. *Planta* **237**: 173–187.

Kabel MA, van den Borne H, Vincken JP, Voragen Schols HA. 2007. Structural differences of xylans affect their interaction with cellulose. *Carbohydrate Polymers* **69**: 94–105.

Karimi M, Inzé D, Depicker A. 2002. Gateway vectors for Agrobacterium-mediated plant transformation. *Trends in Plant Science* 7: 193–195.

Kosík O, Garajová S, Matulová M, Rehulka P, Stratilová E, Farkaš V. 2011. Effect of the label of oligosaccharide acceptors on the kinetic parameters of nasturtium seed xyloglucan endotransglycosylase (XET). *Carbohydrate Research* **346**: 357–361.

Kosik O, Bromley JR, Busse-Wicher M, Zhang Z, Duprée P. 2012.. Studies of enzymatic cleavage of cellulose using polysaccharide analysis by carbohydrate gel electrophoresis (PACE). *Methods in Enzymology* **510**: 51–67.

Lafarguette F, Leple JC, Dejardin A, Laurans F, Costa G, Lesage-Descauses MC, Pilate G. 2004. Poplar genes encoding fasciclin-like arabinogalactan proteins are highly expressed in tension wood. *New Phytologist* **164**: 107–121.

Lagerwall JPF, Schütz C, Salajkova M, Noh JH, Park JH, Scalia G, Bergström L. 2014. Cellulose nanocrystal-based materials: from liquid crystal self-assembly and glass formation to multifunctional thin films. *NPG Asia Materials* **6**: e80

Landrein B, Hamant O. 2013. How mechanical stress controls microtubule behavior and morphogenesis in plants: history, experiments and revisited theories. *Plant Journal* **75**: 324–338.

Larsson M, Gräslund S, Yuan L, Brundell E, Uhlén M, Höög C, Ståhl S. 2000. High-throughput protein expression of cDNA products as a tool in functional genomics. *Journal of Biotechnology* **80**: 143–157.

Latha Gandla M, Derba-Maceluch M, Liu X, Gerber L, Master ER, Mellerowicz EJ, Jönsson LJ. 2014. Expression of a fungal glucuronoyl esterase in *Populus*: effects on wood properties and saccharification efficiency. *Phytochemistry*, in press.

Lee C, Teng Q, Huang W, Zhong R, Ye ZH. **2011.** Molecular dissection of xylan biosynthesis during wood formation in poplar. *Molecular Plant* **4**: 730–747.

Leppänen K, Bjurhager I, Peura M, Kallonen A, Suuronen JP, Penttilä P, Love J, Fagerstedt K, Serimaa R. 2011. X-ray scattering and microtomography study on the structural changes of never-dried silver birch, European aspen and hybrid aspen during drying. *Holzforschung* **65**: 865–873.

Lever M. 1972. A new reaction for colorimetric determination of carbohydrates. *Analytical Biochemistry* **47**: 273–279.

Li S, Lei L, Somerville C, Gu Y. 2012. Cellulose synthase interactive protein1 (CSI1) links microtubules and cellulose synthase complexes. *Proceeding of the National Academy of Sciences of the United States of America* **109**: 185–190.

Li XL, SpánikováS, de Vries RP, Biely P. 2007. Identification of genes encoding microbial glucuronoyl esterases. *FEBS Letters* **581**: 4029–4035.

Lindeboom JJ, Nakamura M, Hibbel A, Shundyak K, Gutierrez R, Ketelaar T, Emons AMC, Mulder BM, Kirik V, Ehrhardt DW. 2013. A mechanism for reorientation of cortical microtubule arrays driven by microtubule severing. *Science* **342**: 1245533.

Livak KJ, Schmittgen TD. 2001. Analysis of relative gene expression data using real-time quantitative PCR and the $2^{(-\text{Delta Delta C(T)})}$ method. *Methods* **25**: 402–408.

MacMillan CP, Mansfield SD, Stachurski ZH, Evans R, Southerton SG. 2010. Fasciclin-like arabinogalactan proteins: specialization for stem biomechanics and cell wall architecture in Arabidopsis and *Eucalyptus*. *Plant Journal* **62**: 689–703.

McCartney L, Blake AW, Flint J, Bolam DN, Boraston AB, Gilbert HJ, Knox JP. 2006. Differential recognition of plant cell walls by microbial xylan-specific carbohydrate-binding modules. *Proceeding of the National Academy of Sciences of the United States of America* **103**: 4765–4770.

Mellerowicz EJ, Baucher M, Sundberg B, Boerjan W. 2001. Unravelling cell wall formation in the woody dicot stem. *Plant Molecular Biology* **47**: 239–274.

Mellerowicz EJ, Sundberg B. 2008. Wood cell walls: biosynthesis, developmental dynamics and their implications for wood properties. *Current Opinion in Plant Biology* **11**: 293–300.

Mellerowicz EJ, Gorshkova T. 2012. Tensional stress generation in gelatinous fibres: a review and possible mechanism based on cell wall structure and composition. *Journal of Experimental Botany* **63**: 551–565.

Minic Z, Jouanin L. 2006. Plant glycoside hydrolases involved in cell wall polysaccharide degradation. *Plant Physiology and Biochemistry* **44**: 435–449.

Naran R, Black S, Decker SR, Azadi P. 2009. Extraction and characterization of native heteroxylans from delignified corn stover and aspen. *Cellulose* **16**: 661–675.

Paolillo Jr DJ, Rubin G. 1991. Relative elemental rates of elongation and the protoxylem-metaxylem transition in hypocotyls of soybean seedlings. *American Journal of Botany* **78**: 845–854.

Paull RE, Chen NJ. 1983. Postharvest variation in cell wall-degrading enzymes of papaya (*Carica papaya* L.) during fruit ripening. *Plant Physiology* **72**: 382–385.

Reis D, Vian B, Chanzy H, Roland JC. 1991. Liquid crystal-type assembly of native cellulose-glucuronoxylans extracted from plant cell wall. *Biology of the Cell* **73**: 173–178.

Reis D, Vian B. 2004. Helicoidal pattern in secondary cell walls and possible role of xylans in their construction. *Comptes Rendus Biologies* **327**: 785–790.

Rennie EA, Scheller HV. 2014. Xylan biosynthesis. *Current Opinion in Biotechnology* **26**:100–107.

Rogowski A, Baslé A, Farinas CS, Solovyova A, Mortimer JC, Dupree P, Gilbert HJ, Bolam DN. 2014. Evidence that GH115 α-glucuronidase activity, which is required to degrade plant biomass, is dependent on conformational flexibility. *The Journal of Biological Chemistry*: **289**: 53–64.

Ruel K, Chevalier-Billosta V, Guillemin F, Sierra JB, Joseleau JP. 2006. The wood cell wall at the ultrastructural scale – formation and topochemical organization Maderas. *Ciencia y tecnología* **8**: 107–116.

Scheller HV, Ulvskov P. 2010. Hemicelluloses. *Annual Review of Plant Biology* **61**: 263–289.

Simpson DJ, Fincher GB, Huang AHC, Cameron-Mills V. 2003. Structure and function of cereal and related higher plant (1 → 4)-beta-xylan endohydrolases. *Journal of Cereal Science* **37**: 111–127.

Sjödin A, Bylesjö M, Skogström O, Eriksson D, Nilsson P, Rydén P, Jansson S, Karlsson J. 2006. UPSC-BASE - *Populus* transcriptomics online. *Plant Journal* **48**: 806–817.

Slade AM, Hoj PB, Morrice NA, Fincher GB. 1989. Purification and characterization of three (1→4)-ß-D-xylan endohydrolases from germinated barley. *European Journal of Biochemistry* **185**: 533–539.

Spániková S, Biely P. 2006. Glucuronoyl esterase – novel carbohydrate esterase produced by *Schizophyllum commune. FEBS Letters* **580**: 4597–4601.

Spániková S, Polakova M, Joniak D, Hirsch J, Biely P. **2007.** Synthetic esters

recognized by glucuronoyl esterase from Schizophyllum commune. *Archives of Microbiology* **188**: 185–189.

Sterky F, Bhalerao RR, Unneberg P, Segerman B, Nilsson P, Brunner AM, Campaa L, Jonsson LJ, Tandre K, Strauss SH *et al.* 2004. A *Populus* EST resource for plant functional genomics. *Proceeding of the National Academy of Sciences of the United States of America* **101**: 13951–13956.

Stevanic JS, Salmén. 2009. Orientation of the wood polymers in the cell wall of spruce wood fibres. *Holzforschung* **63**: 497–503.

Stewart D, Yahiaoui N, McDougall GJ, Myton K, Marque C, Boudet AM, Haigh J. 1997. Fourier-transform infrared and Raman spectroscopic evidence for the incorporation of cinnamaldehydes into the lignin of transgenic tobacco (*Nicotiana tabacum* L.) plants with reduced expression of cinnamyl alcohol dehydrogenase. *Planta* **201**: 311–318.

Svedström K, Lucenius J, Van den Bulcke J, Van Loo D, Immerzeel P, Suuronen J-P, Brabant L, Van Acker J, Saranpää P, Fagerstedt K et al. 2012. Hierarchical structure of juvenile hybrid aspen xylem revealed using x-ray scattering and microtomography. *Trees-Structure and Function* **26**: 1793–1804.

Suen DF, Huang AHC. 2006. Maize pollen coat xylanase facilitates pollen tube penetration into silk during sexual reproduction. *Journal of Biological Chemistry* **282**: 625–636.

Suzuki M, Kato A, Nagata N, Komeda Y. 2002. A Xylanase, AtXyn1, is predominantly expressed in vascular bundles, and four putative xylanase genes were identified in the *Arabidopsis thaliana* genome. *Plant and Cell Physiology* **43**: 759–767.

Takahashi J, Rudsander UJ, Hedenström M, Banasiak A, Harholt J, Amelot N, Immerzeel P, Ryden P, Endo S, Ibatullin FM *et al.* 2009. *KORRIGAN1* and its aspen homolog *PttCel9A1* decrease cellulose crystallinity in Arabidopsis stems. *Plant and Cell Physiology* **50**: 1099–1115.

Teleman A, Lundqvist J, Tjerneld F, Stålbrand H, Dahlman O. 2000. Characterization of acetylated 4-*O*-methylglucuronoxylan isolated from aspen employing 1H and 13C NMR spectroscopy. *Carbohydrate Research* **329**: 807–815.

Theander O, Westerlund EA. 1986. Studies on dietary fiber. 3. Improved procedures for analysis of dietary fiber. *Journal of Agricultural and Food Chemistry* **34**: 330−336.

Timell TE. 1967. Recent progress in the chemistry of wood hemicellulose. *Wood Science and Technology* **1**: 45–70.

Trygg J, Wold S. 2002. Orthogonal projections to latent structures (O-PLS). *Journal of Chemometrics* **16**: 119–128.

Van Campenhout S, Pollet A, Bourgois TM, Rombouts S, Beaugrand J, Gebruers K, De Backer E, Courtin CM, Delcour JA, Volckaert G. 2007. Unprocessed barley aleurone endo-β-1,4-xylanase X-I is an active enzyme. *Biochemical and Biophysical Research Communications* **356**: 799–804.

Vandesompele J, De Preter K, Pattyn F, Poppe B, Van Roy N, De Paepe A, Speleman F. 2002. Accurate normalization of real-time quantitative RT-PCR data by geometric averaging of multiple internal control genes. *Genome Biology* **3**: research 34, PMID:12184808.

Wightman R, Chomicki G, Kumar M, Carr P, Turner SR. 2013. SPIRAL2 determines plant microtubule organization by modulating microtubule severing. *Current Biology* **23**: 1902–1907.

Wilkins O, Nahal H, Foong J, Provart NJ, Campbell MM. 2009. Expansion and diversification of the *Populus* R2R3-MYB family of transcription factors. *Plant Physiology* **149**: 981–993.

Winzéll A, Aspeborg H, Wang Y, Ezcurra I. 2010. Conserved CA-rich motifs in gene promoters of PtxtMYB021-responsive secondary cell wall carbohydrate-active enzymes in *Populus*. *Biochemical and Biophysical Research Communications* **394**: 848–853.

Wu SSH, Suen DF, Chang HC, Huang AHC. 2002. Maize tapetum xylanase is synthesized as a precursor, processed and activated by a serine protease, and deposited on the pollen. *Journal of Biological Chemistry* **277**: 49055–49064.

Yamamoto H, Ruelle J, Arakawa Y, Yoshida M, Clair B, Gril J. 2010. Origin of the characteristic hygro-mechanical properties of the gelatinous layer in tension wood from Kunugi oak (*Quercus acutissima*). *Wood Science and Technology* **44**: 149–163.

Yoneda A, Ito T, Higaki T, Kutsuna N, Saito T, Ishimizu T, Osada H, Hasezawa S, Matsui M, Demura T. 2010. Cobtorin target analysis reveals that pectin functions in the deposition of cellulose microfibrils in parallel with cortical microtubules. *Plant Journal* **64**: 657–667.

Zhong R, Morrison III WH, Himmelsbach DS, Poole II FL, Ye ZH. **2000.** Essential role of caffeoyl coenzyme A *O*-methyltransferase in lignin biosynthesis in woody poplar plants. *Plant Physiology* **124**: 563–577.

Supporting Information:

Fig. S1. Clarification of Phytozome gene models for *PtXyn10A* and *PtXyn10H.*

Fig. S2. Phylogenetic analysis of the GH10 family in *Populus trichocarpa* and *Arabidopsis thaliana*.

Fig. S3. *PtxtXyn10A* expression analyses.

Fig. S4. *Populus* GH10 family gene expression analysis.

Fig. S5. Effects of *PtxtXyn10A* expression on wood anatomy and ultrastructure.

Fig. S6. Relationship between wood cell dimensions, volumetric mass and expression level of *PtxtXyn10A*.

Supplemental Tables:

Table S1. GH10 gene models of *P. trichocarpa*, v 7.0 (http://www.phytozome.net/).

Table S2. Size-exclusion chromatography parameters of hemicellulose distributions in the transgenic antisense lines and WT.

Table S3. List of genes significantly ($P \leq 0.05$ and $B \geq 0$) downregulated in both transgenic antisense lines 2 and 32.

Table S4. List of genes significantly ($P \leq 0.05$ and $B \geq 0$) upregulated in both transgenic antisense lines 2 and 32.

Table S5. List of primers used for RT-qPCR analysis.

Table S6. List of primers used for cloning.

Fig. captions

Fig. 1. *Ptxt*Xyn10A protein accumulates in cell walls.

(a) Modular structure of *Ptxt*GT10A showing three carbohydrate-binding modules 22 (CBM22) and a catalytic domain (Xyn10). Predicted *N*-glycosylation sites are marked, along with the predicted processing site shown by an arrow.

(b) Western blotting of soluble and cell wall bound protein fractions extracted from developing xylem and apical bud tissues and probed with the antibody Kamisa raised against the C-terminal fragment of *Ptxt*Xyn10A. A 68 kDa peptide (arrow) was detected in the cell wall bound protein fraction from developing xylem.

(c) Immunolocalisation of *Ptxt*Xyn10A protein fused with eGFP and stably expressed in *Arabidopsis*. The root cells were plasmolyzed with 20% v/v mannitol, fixed, immunolabelled against GFP protein and observed by confocal microscopy. The arrowhead shows the signal from cell wall and the arrow shows the plasmolysed protoplast. The negative control was assay without primary antibodies. Bar = 20 μm.

Fig. 2. Xylanase and xylan endotransglycosylase activities are present in cell wall bound protein fractions extracted from developing xylem.

(a) Xylanase and xylan endotransglycosylase activities detected by thin-layer chromatography of products after incubation of extracted proteins with xylohexaose ($Xylo_6$) at either 1.25 mM or 6.25 mM concentrations, as indicated in the figure, for 1-42 h at 40°C. Extracts boiled for 10 min were used as negative controls. At low substrate concentration, the main products had DP 1-5, indicating hydrolysis, whereas at high substrate concentration, products corresponding to DP 8-10 were additionally detected, indicating xylan endotransglycosylase activity. The DP of xylooligosaccharides was determined from standards containing $Xylo_1$ to $Xylo_6$ either directly (black triangles) of by interpolation (white triangles). Volumes corresponding to the same amounts of substrates were loaded in each lane.

(b) Xylan endotransglycosylation activity detected by ANTS assay as described in the Material and Methods. The SE bars show variability among technical replicates. The control reaction lacked protein extracts.

995 (c) Susceptibility of fluorescent product detected by ANTS assay for 1 h incubations with
996 pectate lyase (PL), xylanase M1 (XylM1) or buffer (Buf; no enzymatic treatment) at
997 40°C.

998 **Fig. 3.** Expression of *Ptxt*Xyn10A in *Arabidopsis* protoplasts results in strong
999 upregulation of xylan endotransglycosylase but not xylanase.

1000 Protoplasts were transfected with either Xyn10A or an empty vector, and transgene
1001 expression was verified by RT-qPCR. Mean enzymatic activity ± SE, *n*=4 biological
1002 replicates, *P* values correspond to the probability of the null hypothesis in the Fisher test.

1003 (a) Xylan endotransglycosylase specific activities determined by ANTS assay as
1004 described in the Material and Methods.

1005 (b) Xylanase specific activities determined by Azo-Xylan solubilisation.

1006 (c) Xylanase specific activity determined by the formation of reducing ends.

1007 **Fig. 4**. Downregulation of *Ptxt*Xyn10A reduces xylan endotransglycosylase activity in
1008 developing wood. Three independent transgenic antisense lines (2, 3 and 32) are
1009 compared to WT.

1010 (a) *PtxtXyn10*A transcript levels in transgenic antisense lines and WT determined by RT-
1011 qPCR. Data were calibrated to CYP and normalized to the WT level. Means of 3-9
1012 biological replicates ± SE.

1013 (b) *Ptxt*Xyn10A protein levels detected by the antibody Kamisa in the cell wall bound
1014 protein extracts. The signal from an unrelated cell wall localised protein (*Ptxt*Cel9B3)
1015 was used as a loading control for the transgenic antisense lines.

1016 (c) Xylan endotransglycosylase activity in cell wall bound protein extracts from the
1017 transgenic antisense lines and WT. Means of 3 biological replicates ± SE.

1018 (d) Xylanase activity in transgenic antisense lines determined by the formation of
1019 reducing ends following incubation of the cell wall bound protein extracts with xylan.
1020 Means of three biological replicates ± SE. The effect of genotype was not significant
1021 (ANOVA, $P \leq 10\%$).

1022 * indicates values significantly different from WT (*t*-test, 5%)

Fig. 5. Downregulation of *PtxtXyn10A* increases plant primary growth.

Stem height, diameter, number of internodes, internode length, leaf length and width were measured in trees after three months of growth in the greenhouse. Average cell surface area was determined for the leaf adaxial epidermis from nail polish casts. Means of ten biological replicates ± SE. * indicates values significantly different from WT (*t*-test, 5%).

Fig. 6. Glucuronoxylan [Me]GlcA substitution pattern in transgenic antisense lines with reduced xylan endotransglycosylase activity (2 and 3) and in wild-type aspen (WT).

Milled wood was hydrolysed with *Bo*GH30 to completion and the resulting digestion products were analysed using polysaccharide analysis by carbohydrate gel electrophoresis (PACE). Standards X1 to X6 (S), enzyme (E only) and wood material only (no E) are shown. * indicates non-specific labelling product.

Fig. 7. OPLS-DA models of diffuse reflectance Fourier-transform infrared spectra.

(a) Scores plot showing the separation of transgenic antisense plants (empty symbols; squares: line 2, triangles: line 3, diamonds: line 32) from wild type (filled dots), using five to six individual plants per line.

(b) Corresponding loadings plot showing factors responsible for the separation. Bands that are referred to in the text are labelled. Bands that are positive (*i.e.* more intense in the transgenic antisense lines) are labelled with black regular fonts, bands that are negative (*i.e.* more intense in the wild type) are labelled with black italic fonts. The 1595 cm^{-1} band was unchanged and is labelled with grey regular font. The model has the following details: 1 + 1 components (predictive + orthogonal), R2X(cum) = 0.642, R2Y(cum) = 0.598; Q2(cum)= 0.254.

Fig. 8. Suppression of *PtxtXyn10A* affects orientation of cellulose microfibrils in secondary walls of wood fibres.

(a) Orientation of slit-pits relative to fibre axis in isolated wood fibres from transgenic antisense lines and WT visualized using Nomarski optics. Example of slit pits and their angle is shown beside the graph.

(b) Cellulose microfibril angle (MFA) measured by X-ray diffraction in samples from transgenic antisense lines and WT representing primarily normal wood after exclusion of tension wood samples based on crystallite size.

For (a) and (b) Means of 3 biological replicates ± SE. The *P* value for the difference between both transgenic antisense lines and the WT is indicated above the line.

(c) Appearance of cellulose microfibrils in the transgenic antisense line 2, 3 and WT visualised by SEM. The fibres were oriented vertically and observed from the inside. The cell wall appearance was similar in the transgenic antisense lines and WT, but the microfibril angle (traced with white lines) was larger in the WT. Scale bar = 200 nm.

Fig. 9. Proposed hypothesis of *Ptxt*Xyn10A action on cellulose microfibril angle.

The main function of *Ptxt*Xyn10A is proposed to be the elimination of tension in cell wall that arises during cell wall assembly. The suppression of *Ptxt*Xyn10A causes the build-up of tension in the cell wall, which is sensed by mechanical sensors (tension gated Ca^{++} channels, and/or receptor leucine-rich kinases) that activate the mechanosensing signal transduction pathway, causing re-organization of cortical microtubules and subsequent re-orientation of cellulose microfibrils.

Tables:

Table 1. Sugar composition and lignin content in the transgenic antisense lines and WT. Five trees were pooled per line, two technical replicates. Neutral sugar and lignin contents are expressed as % of the total measured yield. The yield was over 865 mg/g.

Line	Ara	Gal	Glc	Xyl	Man	Klason lignin	Acid soluble lignin	Total lignin
	%	%	%	%	%	%	%	%
2	0.32	1.15*	51.6*	18.8*	3.01*	20.9*	4.20*	25.1*
3	0.35	1.08*	51.5*	19.7*	3.07	19.8*	4.43*	24.3*
32	0.32	1.17*	51.8*	19.3*	2.94	19.9*	4.45*	24.4*
WT	0.35	1.69	54.3	18.1	2.51	19.0	4.09	23.0
$P_{\text{WT vs. Xyn10A AS}}$[1]	0.620	0.004	0.001	0.001	0.049	0.001	0.001	0.001

* $P \leq 5\%$ (*t* test);

[1] $P_{\text{WT vs. Xyn10A AS}}$ values correspond to the difference between all transgenic lines and the WT.

Table 2. Cell wall and stress signalling related transcripts significantly affected in both transgenic antisense lines, 2 and 32, as compared to the WT.

Class	Gene	Annotation	M value		Closest
			2	32	*A. thaliana*
pectins	Potri.014G004500	Rhamnogalacturonate lyase family protein	-2.487	-0.880	AT2G22620
	Potri.010G152000	polygalacturonase *Pt*GH28_75	0.749	0.895	AT1G48100
	Potri.003G156600	similar to GALACTAN SYNTHASE 2	-2.472	-0.805	AT5G44670
	Potri.001G052300	pectate lyase *Pt*PL1_26	0.604	1.072	AT4G13710
	Potri.015G087800	similar to probable pectate lyase 22	0.491	1.077	AT5G63180
xylan	Potri.008G108100	similar to beta-D-xylosidase	1.049	0.841	AT5G49360
xyloglucan	Potri.018G095100	*Pt*XTH16_17	-0.835	-0.884	AT4G25810
	Potri.017G101300	O-fucosyltransferase family protein	-1.839	-0.637	AT5G15740
mannan	Potri.013G130400	similar to ENDO-BETA-MANNASE 2	1.363	1.037	AT2G20680
AGP	Potri.013G151300	fasciclin-like AGP *Pt*FLA12K	-2.692	-1.097	AT5G60490
	Potri.012G015000	similar to fasciclin-like FLA 11	-1.942	-1.005	AT5G03170
	Potri.009G012200	fasciclin-like AGP *Pt*FLA12V	-1.786	-0.878	AT5G60490
	Potri.013G151500	fasciclin-like AGP *Pt*FLA12J	-2.138	-1.179	AT5G60490
	Potri.019G123200	similar to fasciclin-like FLA 11	-2.187	-1.157	AT5G03170
	Potri.015G013300	fasciclin-like AGP *Pt*FLA12E or F	-2.090	-1.236	AT5G03170
	Potri.009G012100	fasciclin-like AGP *Pt*FLA12G, P or Q	-2.242	-1.313	AT5G03170
	Potri.001G450200	beta-galactosyltransferase *Pt*GT31_32	-1.286	-0.617	AT1G32930
	Potri.013G151400	similar to fasciclin-like FLA 11	-2.293	-1.174	AT5G03170
	Potri.006G144500	Similar to glycosyl hydrolase family 35	0.588	0.557	AT3G13750
	Potri.005G161100	similar to AGP5	-1.109	-0.705	AT1G35230
cellulose	Potri.002G034000	Fruktokinase	-2.399	-0.729	AT1G19600
	Potri.004G117200	similar to COBRA like COBL4	-2.845	-0.971	AT5G15630
	Potri.003G151700	similar to KORRIGAN1 *Pt*Cel9A1	-1.436	-0.727	AT5G49720
lignin	Potri.008G038200	phenylalanine ammonia-lyase1 (PAL1)	1.333	0.752	AT2G37040
	Potri.018G100500	cinnamoyl-CoA reductase related	1.147	0.598	AT2G23910
microtubule	Potri.008G139700	microtubule associated MAP65-like	1.795	1.214	AT2G01910
	Potri.014G088500	similar to *At*MPK4	0.745	0.783	AT4G01370
	Potri.006G018000	similar to *At*MAP70-5	1.443	1.383	AT4G17220
LRK	Potri.008G140500	Similar to BRL2	0.816	0.550	AT2G01950
	Potri.012G128700	Leucine-rich repeat protein kinase family protein	0.739	0.992	AT5G51560
	Potri.019G122700	Leucine-rich repeat receptor-like protein kinase family protein;	-1.469	-0.556	AT4G08850
calcium	Potri.001G005500	Calcium binding protein involved in cryptochrome and phytochrome coaction	1.624	1.495	AT4G08810
	Potri.016G049100	CaLB domain, plant phosphoribosyltransferase family protein	0.861	0.858	AT3G57880
	Potri.009G052700	similar to calcium-dependent protein kinase 1; MSCK1	0.899	0.651	AT5G12480
vesicle	Potri.001G278800	clathrin heavy chain	2.885	2.942	AT3G11130
ethylene, stress	Potri.017G108800	similar to S-adenosylmethionine decarboxylase.	-2.343	-1.119	AT3G02470
	Potri.013G044100	ethylene receptor EIN4-like	1.184	1.134	AT3G04580
	Potri.014G159000	similar to ACC oxidase	-1.038	-1.225	AT1G05010
	Potri.002G078600	similar to ACC oxidase	-2.125	-1.168	AT1G77330
	Potri.004G003000	similar to ACC oxidase	-1.193	-0.706	AT1G05010

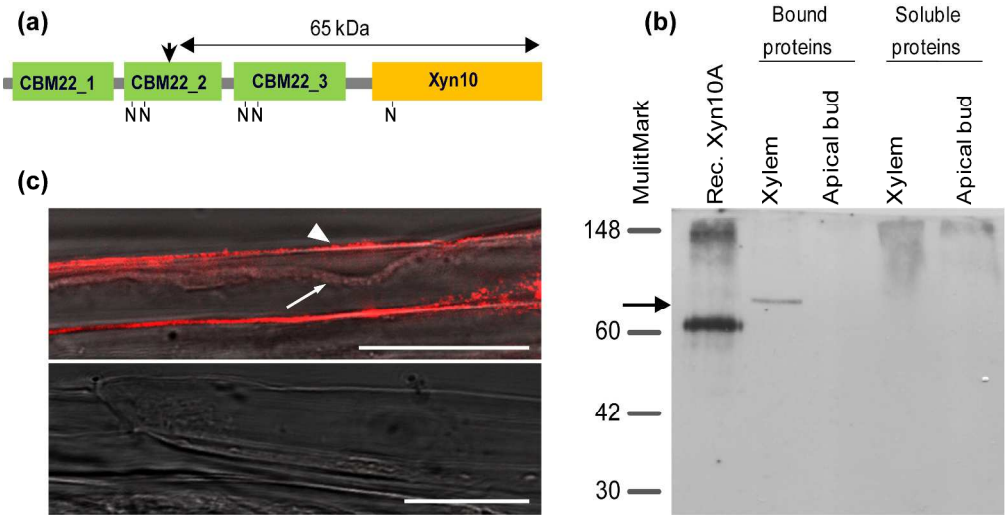

330x169mm (300 x 300 DPI)

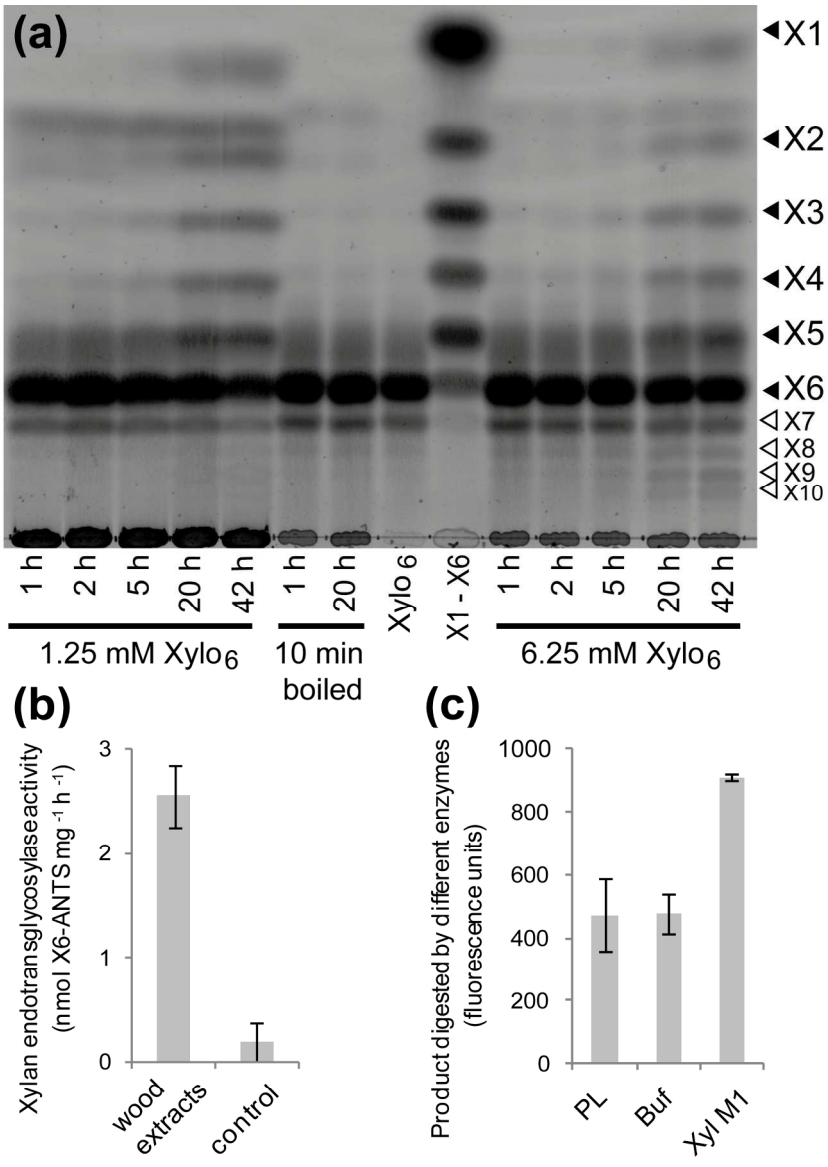

157x226mm (300 x 300 DPI)

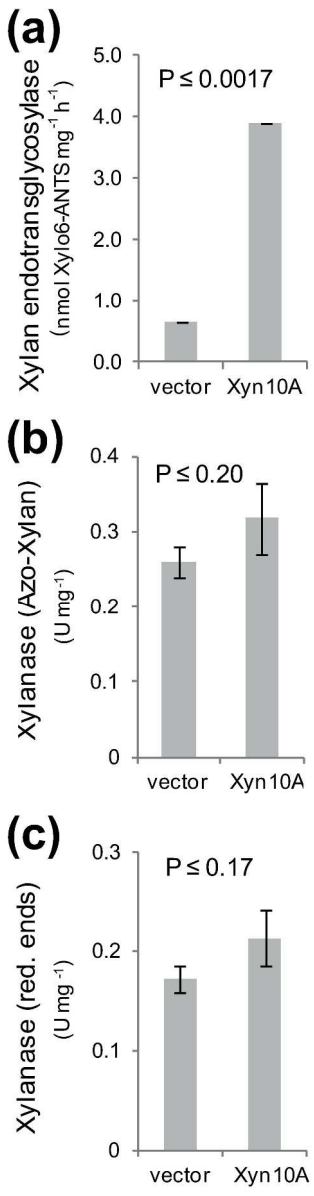

221x748mm (300 x 300 DPI)

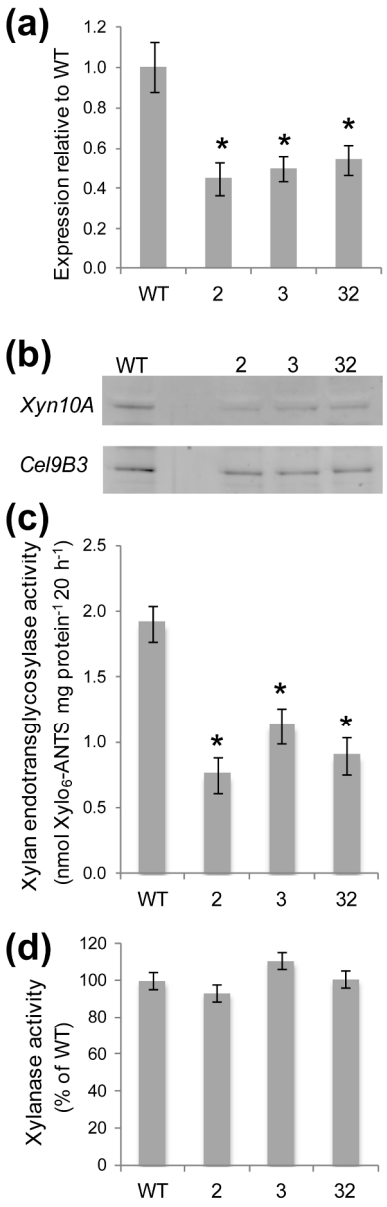

99x273mm (300 x 300 DPI)

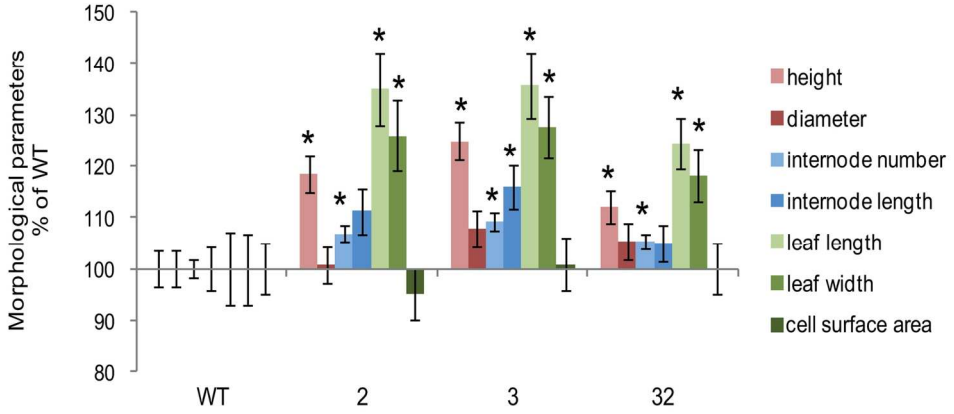

149x66mm (300 x 300 DPI)

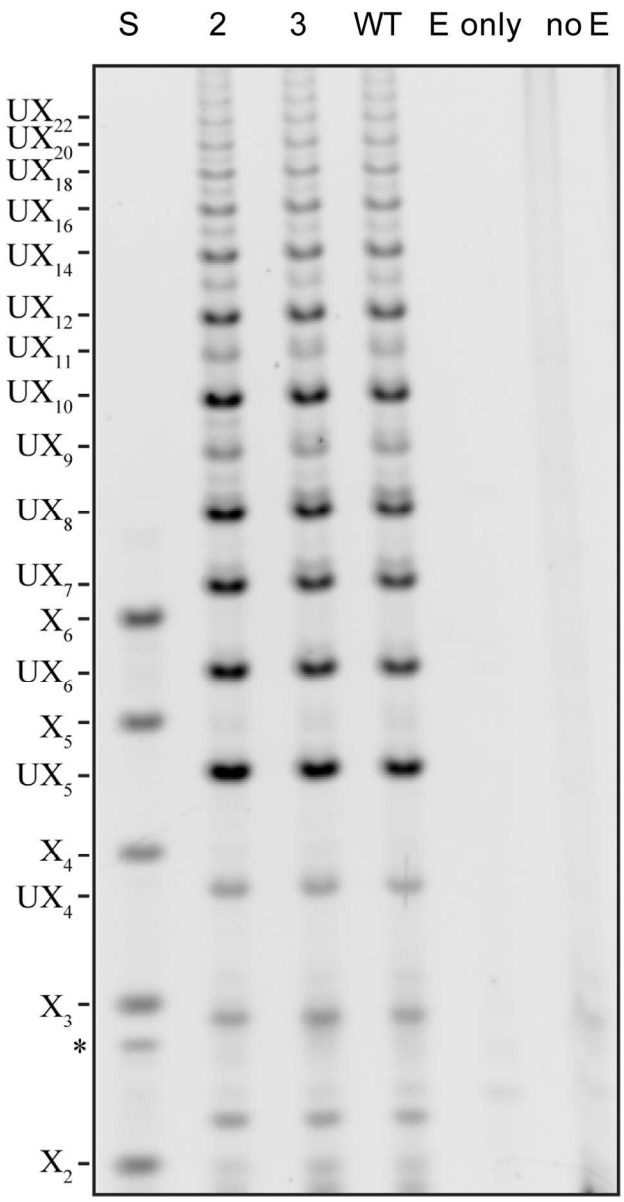

95x184mm (300 x 300 DPI)

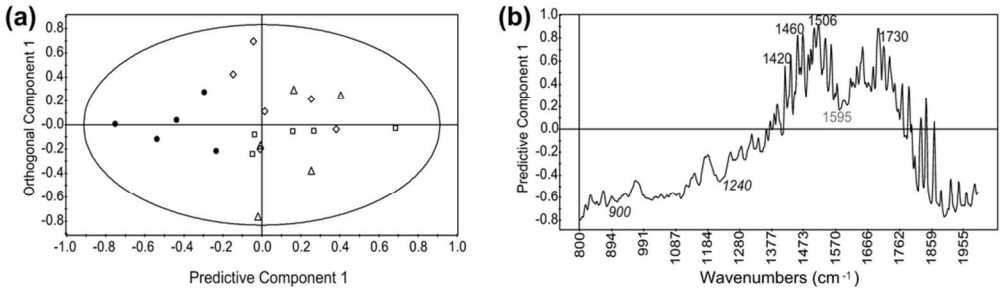

92x26mm (300 x 300 DPI)

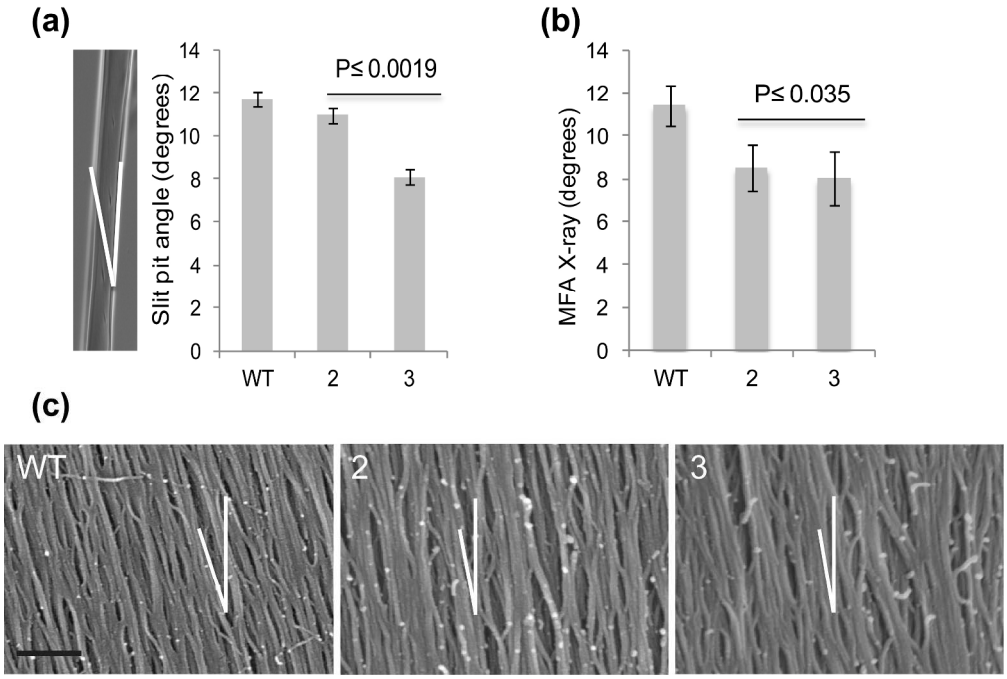

261x175mm (300 x 300 DPI)

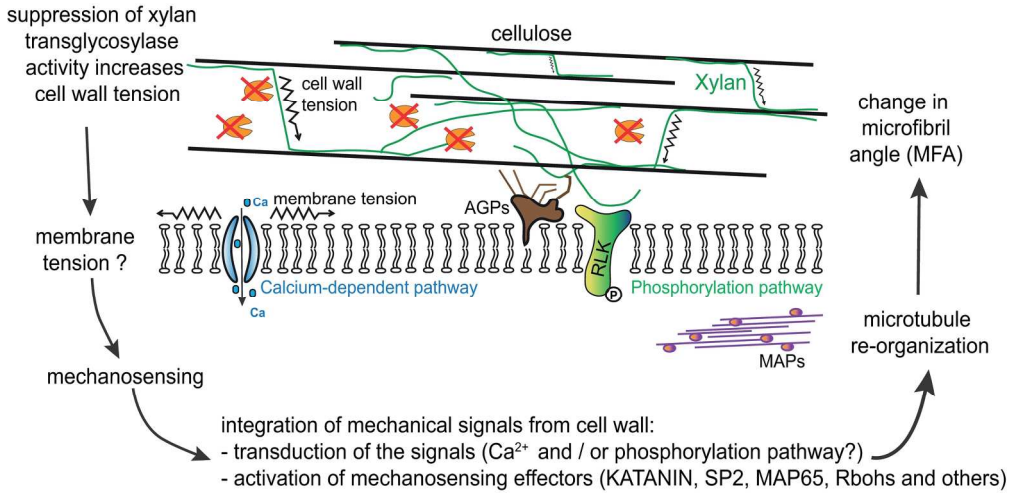

189x92mm (300 x 300 DPI)